Effects of Chlorine and Alkali Chlorides on Corrosion of Silicon Carbide Based Ceramics in Combustion Environments

M.J. McNallan, S.Y. Ip, C. Park, S.Y. Lee, P.P. Hsu and Y.S. Park

CEMM Department, m/c 246, University of Illinois at Chicago
842 W. Taylor St., Chicago, IL 60607, U.S.A.

ABSTRACT

Silicon carbide based engineering ceramics are used in high temperature furnaces as structural and heat exchanger components. Chlorine or alkali chloride contamination may be present in waste incineration or chemical treatment environments in such furnaces. The effects of these contaminants on the corrosion and oxidation resistance of silicon carbide based ceramics is discussed from the standpoint of understanding the chemical mechanisms of attack and predicting the conditions under which unacceptable degradation can occur.

I. INTRODUCTION

Silicon based non-oxide ceramics such as silicon carbide and silicon nitride have many applications in high temperature industrial furnaces at temperatures exceeding 1000°C. The high temperature strength and creep resistance of these materials are superior to those of competitive nickel based superalloys and intermetallic materials, and the thermal conductivity and thermal shock resistance of silicon based non-oxide ceramics are superior to those of the oxide refractory ceramics which have traditionally been used at temperatures above the capabilities of metals.

These materials can be particularly useful in extending the operating temperatures of heat exchangers and fossil fuel fired industrial furnaces /1/. Because of the high temperatures, the use of silicon carbide based heat exchangers in waste heat recuperators can substantially improve the efficiency of furnace operations in comparison to furnaces which operate without recuperators or with metallic heat exchangers /2/. Other important applications include indirect fired radiant tube burners and high temperature filtration systems. The corrosion experienced by silicon carbide in some complex industrial environments may be a potentially limiting factor for its use in these applications.

Although neither silicon carbide nor silicon nitride is thermodynamically stable in air, silicon based ceramics have excellent oxidation resistance in air because the silicon is oxidized to SiO_2 which forms a protective film on the surface of the ceramic and separates it from the oxidizing environment /3/. Subsequently, the rate of oxidation is controlled by the rate of permeation of oxygen through the silica film. These rates are low at temperatures up to 1300°C /4/. Accelerated corrosion can occur, however, in environments where SiO_2 is not stable or where contaminants are present which can degrade the protective characteristics of the silica layer.

Combustion processes typically operate with excess air, so that more air is added to the combustion chamber than is required to support complete combustion of the fuel. Therefore, the conditions in gas fired combustion systems are usually likely to be sufficiently oxidizing that SiO_2 would be the thermodynamically stable compound of silicon. Chlorine and alkali chloride contaminants can be present in combustion gases from a number of processes using low quality

fuels (such as municipal wastes) or from some chemical or metallurgical processes /5,6/. An important example of a process where such contaminants influence corrosion is in waste heat recuperation from flue gases from gas fired aluminum remelting furnaces where chlorine and alkali chlorides are used to flux and degas the metal /7/.

From the point of view of the furnace operator, such corrosion processes must be understood to enable him to predict the operating lifetimes of ceramic components used in the furnaces. This understanding will enable him to implement corrosion control strategies (materials selection, application of corrosion inhibitors, or modification of operating conditions) to reduce the amount of corrosion damage. There are three principal mechanisms by which the presence of chlorine or alkali chloride compounds can cause accelerated corrosion of SiC based ceramics. Each of these corrosion mechanisms may be dominant under different conditions of temperature and gas composition and different control strategies may be effective depending on the dominant corrosion mechanism. Therefore, they will be discussed in separate sections in this report.

II. ACTIVE CORROSION

A. Introduction

High temperature corrosion by chlorine differs from high temperature corrosion by other oxidizing species because most chloride and oxychloride corrosion products are volatile at elevated temperatures /8/. High temperature corrosion which results in the formation of volatile corrosion products is referred to as active corrosion, because no rate limiting corrosion product scale is formed. Silicon and silicon carbide are attacked rapidly by active corrosion in pure chlorine at temperatures above 900°C with the corrosion obeying a linear reaction rate law and the principal corrosion product being $SiCl_4(g)$ /9,10/. The rate of this corrosion is affected by temperature, gas flow rate past the sample, and the partial pressure of chlorine in the environment.

Because most combustion processes are operated with excess air, oxygen will usually be present in the gases. Although active corrosion of Si, SiC or Si_3N_4 can occur in low pressure oxygen by the formation of SiO(g), the conditions in combustion gases will usually favor the formation of a protective film of SiO_2 /11/. In a mixed environment containing both oxygen and chlorine, the formation of both condensed SiO_2 and volatile $SiCl_4$ are possible. Under these conditions, active corrosion of the SiC via formation of $SiCl_4$ can occur if the SiO_2 fails to form with a dense, protective morphology. The morphology of the SiO_2 oxidation product in mixed oxygen-chlorine atmospheres is affected by the details of the microstructure of the ceramic and the kinetic mechanism of the corrosion reaction.

B. Apparatus and Procedures

Active corrosion of SiC based ceramics in argon-oxygen-chlorine gas mixtures at elevated temperatures was investigated by thermogravimetric analysis using the apparatus shown schematically in Figure 1. The apparatus consists of a furnace, a reaction tube, a gas mixing and purification system, and a balance. The furnace was generally a Kanthal or nichrome wound resistance furnace, but a furnace with molybdenum silicide heating elements was used for some of the higher temperature experiments. The reaction tube was a fused silica tube for most experiments, but a mullite tube was used for some of the higher temperature experiments. The gas mixing and purification system consisted of a series of purification columns, capillary flowmeters, and mixing chambers, which could be used to combine gases containing up to three components. Argon and oxygen were purified by passage through columns of anhydrous calcium sulfate for water removal and Ascarite™ for CO_2 removal. Chlorine (usually supplied as an Ar-3.5%Cl_2 mixture) or HCl was purified by passage through concentrated sulfuric acid for H_2O removal. The gases were mixed in a column packed with pyrex spheres and flowed upwards through the reaction chamber at a controlled flow rate. The balance was a Cahn 2000 electrobalance in most experiments, but in some high temperature experiments the weight change was measured by measuring the change in extension of a fused silica spring using an optical cathetometer. The sample was suspended from

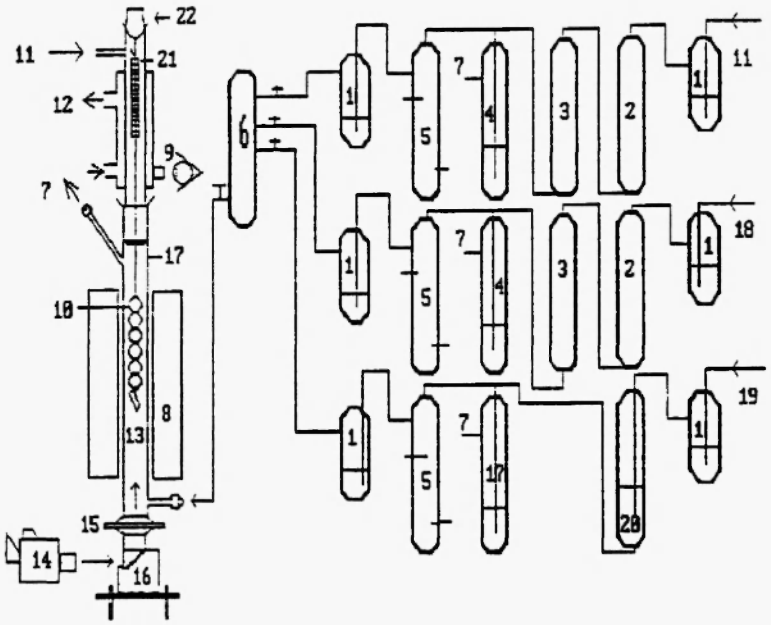

1 BUBBLER	9 CATHETOMETER	17 MULLITE REACTION TUBE
2 DRYLITE COLUMN	10 ALUMINA RINGS	18 OXYGEN CYLINDER
3 ASCARITE COLUMN	11 ARGON GAS	19 CHLORINE GAS CYLINDER
4 DBP COLUMN	12 WATER JACKET	20 CONC. SULFURIC ACID
5 FLOW METER	13 SAMPLE	21 FUSED QUARTZ SPIRAL
6 MIXING COLUMN	14 35mm CAMERA	22 GROUND JOY STICK
7 TO THE HOOD	15 WATCH GLASS	
8 FURNACE	16 PRISM BLOCK	

Fig. 1: Schematic diagram of apparatus used for thermogravimetric experiments.

the weighing mechanism by a fused silica fiber in experiments at temperatures below 1200°C. In experiments at higher temperatures an alumina chain was fabricated to replace the silica fiber in the higher temperature zone of the furnace. Figure 1 shows the high temperature modification of the system.

Test samples were generally flat plates 0.8 - 1.6 mm thick, which were cut from bulk ceramic specimens using a low speed diamond saw. Because most of the engineering ceramics tested in this program were obtained in the form of heat exchanger tubes, most of the test coupons were rings or ring segments cut from the tubing. To begin each experiment, the reaction chamber was purged with purified argon and the sample was suspended from the weighing mechanism and heated to the intended test temperature in an inert atmosphere. When the sample was at the intended test temperature, the experiment was initiated by replacing the inert gas by a reactive mixture flowing at a controlled rate. Decreases in the mass of the specimen indicated formation of volatile corrosion products typical of active corrosion. Increases in the mass of the specimen indicated that condensed corrosion products were forming. The mass of the specimen was measured for a period of 5 to 25 hours depending on the amount of data necessary to characterize the corrosion kinetics. Subsequently, the surfaces of the specimens were examined by optical and scanning electron microscopy to identify the corrosion products and reveal other features of the corrosion process.

C. Effect of Gas Composition on Active Corrosion Kinetics

Consider a particular SiC based ceramic exposed to a high temperature environment containing both oxygen and chlorine. If the chlorine content of the atmosphere is held constant and the oxygen content is continuously increased, the driving force for forming condensed SiO_2 corrosion products will increase with

increasing oxygen content. At low oxygen pressures active corrosion is expected, and at some oxygen content there will be an active to passive transition which will result in a sharp decrease in the overall corrosion rate. Figure 2 shows typical thermogravimetric results for a sintered alpha silicon carbide exposed to gas mixtures which contain 15%HCl or 2%Cl_2 by volume at 900°C. There is virtually no attack of this material in Ar-15%HCl because the chlorine potential in this gas mixture is too low to support formation of $SiCl_4$. When the material is exposed to Ar-2%Cl_2, however, there is significant corrosion which, after a brief induction period, obeys a linear rate equation. When 2%O_2 is added to the gas mixture, the rate of decrease in mass is approximately twice that in the binary argon-chlorine gas mixture. The increase in the corrosion rate occurs because chlorine alone does not effectively remove the carbon component of the SiC owing to the low thermodynamic stability of CCl_4 at elevated temperatures. An atmosphere containing a combination of chlorine and oxygen is more able to react with both components of the ceramic than one containing only chlorine. When the oxygen content of the gas mixture is raised to 20% by volume, sufficient oxygen is present to form a passive SiO_2 film. Under these conditions, the rate of corrosion is again reduced to the point that virtually no attack can be detected. This atmosphere is similar to air with 2% Cl_2 contamination, and a low corrosion rate would be expected for oxidation of SiC in clean air at 900°C. This implies that, when the oxygen content of the gas is sufficiently high to form a passive film, the rate of corrosion of SiC is very low and is not significantly affected by the presence of the chlorine contamination. On the other hand, when the oxygen content is not high enough to form a protective film and active corrosion occurs, the rate of attack is many orders of magnitude higher than would be expected for air oxidation.

During active corrosion in environments containing both oxygen and chlorine, both $SiCl_4$(g) and SiO_2(s) are formed, but the SiO_2 forms with a porous, non-protective morphology. Figure 3 shows an example of a sintered alpha silicon carbide specimen after corrosion in Ar-2%Cl_2-2%O_2, flowing at 6 cm/s at 1000°C. The oxide corrosion product forms as a white ash. X-ray diffraction analysis of the ash indicated that it was amorphous, and EDS microanalysis on the ash detected only silicon, suggesting that it is amorphous SiO_2. Similar porous deposits of amorphous SiO_2 have been

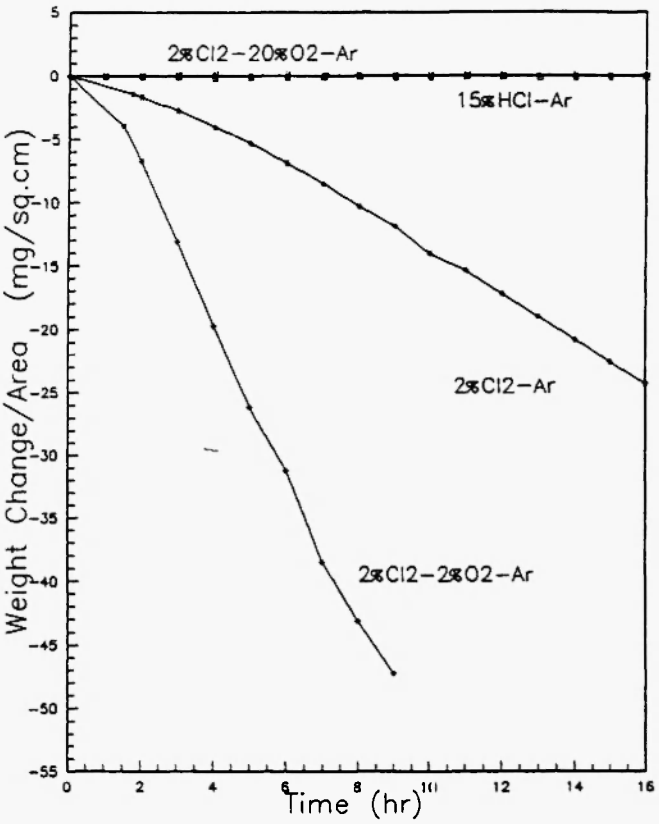

Fig. 2: Thermogravimetric data for sintered alpha silicon carbide in gas mixtures containing 2%Cl_2 at 900°C.

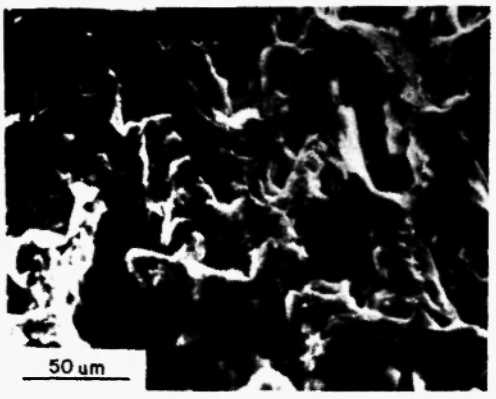

Fig. 3: Scanning electron micrograph of SASC specimen after exposure to Ar-2%Cl_2-2%O_2 at 1000°C.

observed to form during the active oxidation of silicon in low pressure oxygen /12/.

The amount of porous SiO_2 produced in a thermogravimetric experiment can be determined by soaking the specimen in HF after the exposure and measuring the decrease in mass due to etching of the soluble reaction products. Figure 4 shows thermogravimetric results with the mass of SiO_2 indicated by the vertical dashed line at the end of the experiment for a sintered alpha silicon carbide after exposure to four gas mixtures, each containing 2%Cl_2 by volume at 1000°C. Typical active attack is observed in Ar-2%Cl_2. The TGA plot shows a linear decrease in mass, and a small amount of SiO_2 is detected by the etching technique. The addition of 1%O_2 to the gas mixture increases the rate of active oxidation, but does not substantially change the amount of porous oxide produced. The addition of 2%O_2 to the mixture produces approximately the same rate of attack as 1%O_2, but a much larger amount of porous oxide is produced. Very little attack is produced in Ar-2%Cl_2-1%H_2.

Figure 5 shows the thermogravimetric results for the same material in Ar-2%Cl_2 2%O_2 at 1000°C as a function of the velocity of gas flow past the specimen. The rates of attack increase with increasing gas flow rate, and comparison with calculated mass transfer coefficients indicates that the rate of corrosion of SASC in this environment is controlled by mass transfer of the Cl_2 in the gas phase /13/.

D. Active to Passive Transition in Mixed Oxygen-Chlorine Atmospheres

The partial pressure of oxygen at which the active to passive transition occurs can be affected by a number of parameters, including temperature, chlorine pressure, and the microstructure and composition of the ceramic. Because it is very difficult to sinter a covalently bonded ceramic such as SiC to full density, most SiC based

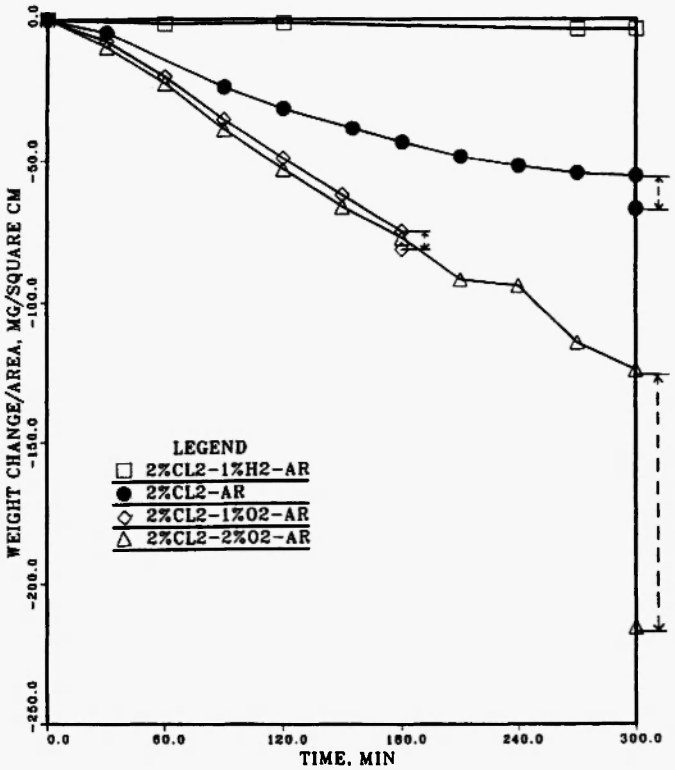

Fig. 4: Thermogravimetric results for SASC exposed to gas mixtures containing 2%Cl_2 at 1000°C showing mass of SiO_2 corrosion products as vertical dashed lines at end of exposure period.

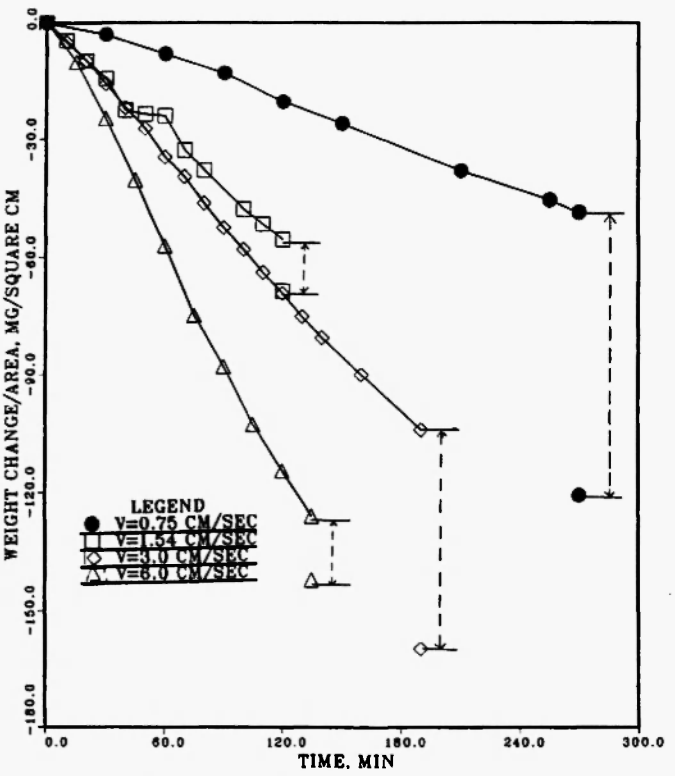

Fig. 5: Thermogravimetric results for SASC in Ar-2%Cl_2-2%O_2 at 1000°C as a function of gas flow rate.

engineering ceramics are not pure SiC but contain various additives to speed sintering. Table I lists the additives and sintering aids in several SiC based engineering ceramics which have been used to manufacture large diameter tubes suitable for use in high temperature heat exchangers. SASC and C-600 are sintered alpha silicon carbide materials containing boron and alumina as sintering aids, respectively. SCRB 205 and CS101K are siliconized silicon carbide materials. These materials contain excess elemental silicon which is liquid at the densification temperature and fills in the porosity in the SiC structure. Although such materials have lower maximum use temperatures than sintered SiC ceramics, they can be used at higher temperatures than metals, and their lower fabrication costs give them advantages over the higher purity materials for many applications.

Figures 6 through 9 show the thermogravimetric results for these four materials in gas mixtures containing 2%Cl_2 and different concentrations of oxygen at 1000°C. The results show a substantial variability in the corrosion kinetics as a function of the sintering aids present in the ceramic and the method used to manufacture it.

As shown in Figure 6, the SASC material is the only one for which the rate of attack increases as the concentration of oxygen increases. Rapid active oxidation is produced in Ar-2%Cl_2, but the rate of attack is higher in gas mixtures containing 1% or 2% O_2 than in Ar-2%Cl_2 to which no oxygen had been added. The rate of attack decreases again when the concentration of oxygen is increased to 4% by volume, but the mode of attack is still consistent with active corrosion. A passive film is formed in Ar-2%Cl_2-20%O_2, and little change in mass is detected in this environment. The material used in the experiments

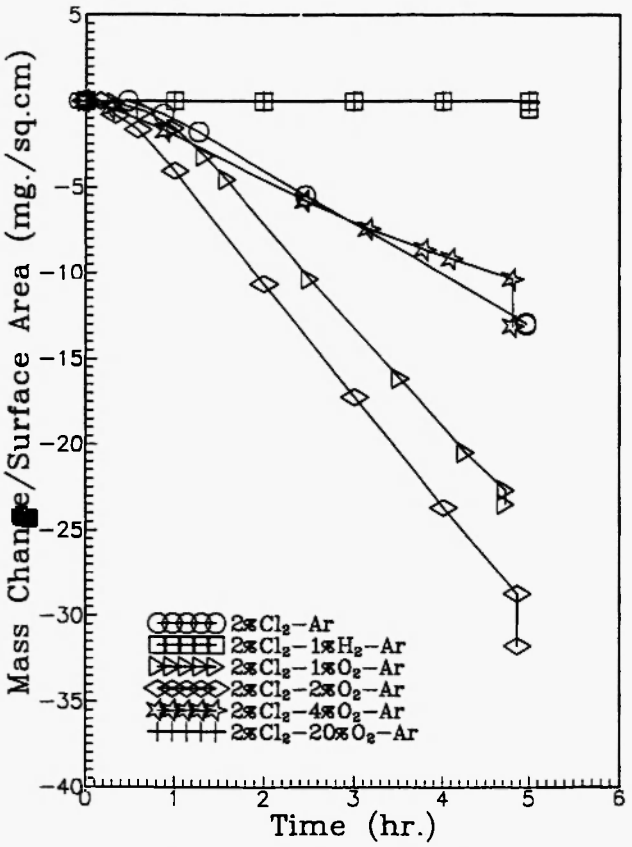

Fig. 6: Thermogravimetric data for SASC in Ar-2%Cl_2O_2 gas mixtures flowing at 1.5 cm/s at 1000°C.

which generated the data presented in Figure 6 is from the same supplier but from a different vintage than that used in the experiments which generated the data presented in Figure 4. Comparison of the differences in these figures indicates that batch to batch variations in the composition and structure of these materials can be sufficient to produce differences in the corrosion behavior in oxygen-chlorine gas mixtures. These

Table 1
Materials in This Study

Material		Sintering Aids	Manufacturer
SASC	Sintered alpha silicon carbide	B, excess C	Carborundum
SCRB 205	Siliconized silicon carbide	Excess Si, Fe	Coors
CS101K	Siliconized silicon carbide	Excess Si	Norton
C-600	Sintered alpha silicon carbide	Aluminum oxide	Asahi

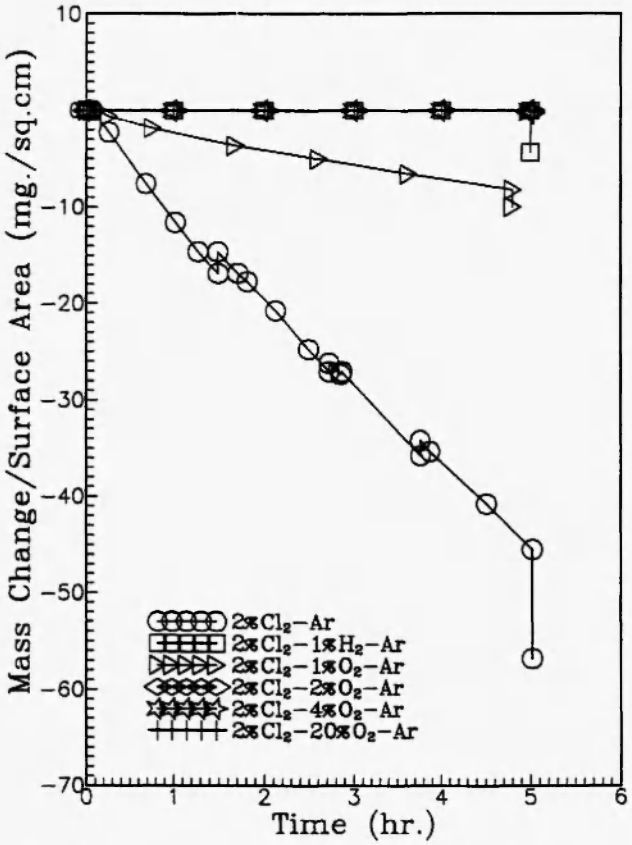

Fig. 7: Thermogravimetric data for C-600 in Ar-2%Cl_2O_2 gas mixtures flowing at 1.5 cm/s at 1000°C.

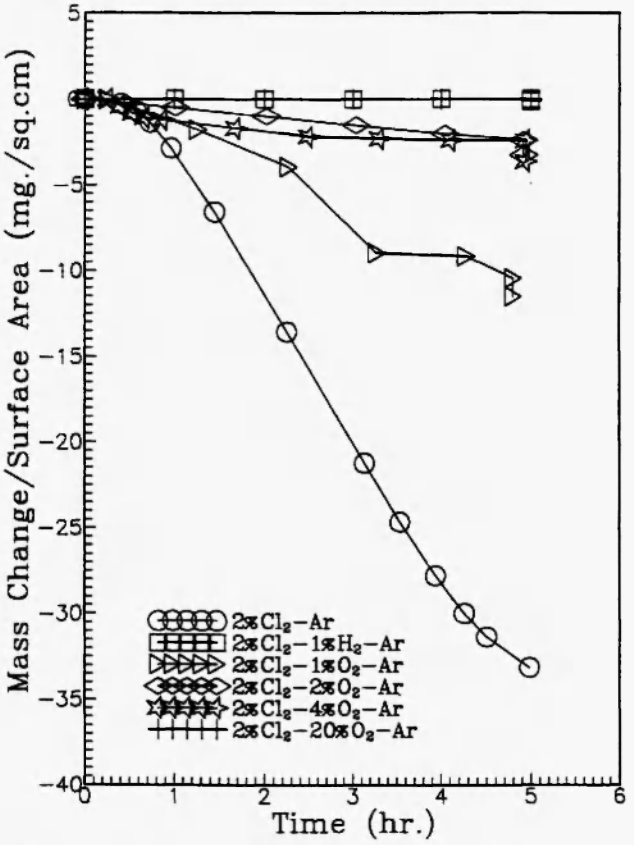

Fig. 8: Thermogravimetric data for SCRB-205 in Ar-2%Cl_2O_2 gas mixtures flowing at 1.5 cm/s at 1000°C.

differences may result from changes in the amount or nature of sintering aids used or in firing procedures.

Figure 7 shows the thermogravimetric results for the C-600 material. The rate of attack of this material in Ar-2%Cl_2 is the highest of any of the four materials tested; however, any addition of oxygen to the gas mixture reduces the rate. A passive film is formed in any mixture containing more than 2%O_2. As was the case with the SASC, no attack is produced in Ar-2%Cl_2-1%H_2. Examination of the surfaces of the corroded specimens by scanning electron microscopy and energy dispersive X-ray microanalysis showed that the attacked surface was covered by porous alumina and silica rich oxidation products.

Figure 8 shows the results for SCRB205. This material is also corroded most rapidly in Ar-2%Cl_2, and any addition of oxygen to the gas mixture reduces the rate of attack. Active corrosion still occurs in gas mixtures containing up to 4% O_2, however, and a passive film is only formed in gas mixtures containing 20%O_2 by volume. Similar behavior is shown in Figure 9 for another siliconized silicon carbide, CS101K. In this case, a passive film forms in the gas mixture containing 4%O_2 by volume. Both of these materials experienced selective attack of the free silicon phase between the SiC grains as shown in Figure 10 for CS101K corroded in Ar-2%Cl_2-1%O_2. This is consistent with earlier results which showed that elemental Si is attacked more rapidly than SiC by chlorine /10/.

The differences in behaviors of the four SiC based materials can be related to the differences in the sintering aids used to fabricate these materials. SASC is sintered with boron and excess carbon. Both of these elements form stable and volatile oxides, and therefore are more likely to be removed from the corroding interface by oxygen than by chlorine. As a result, this

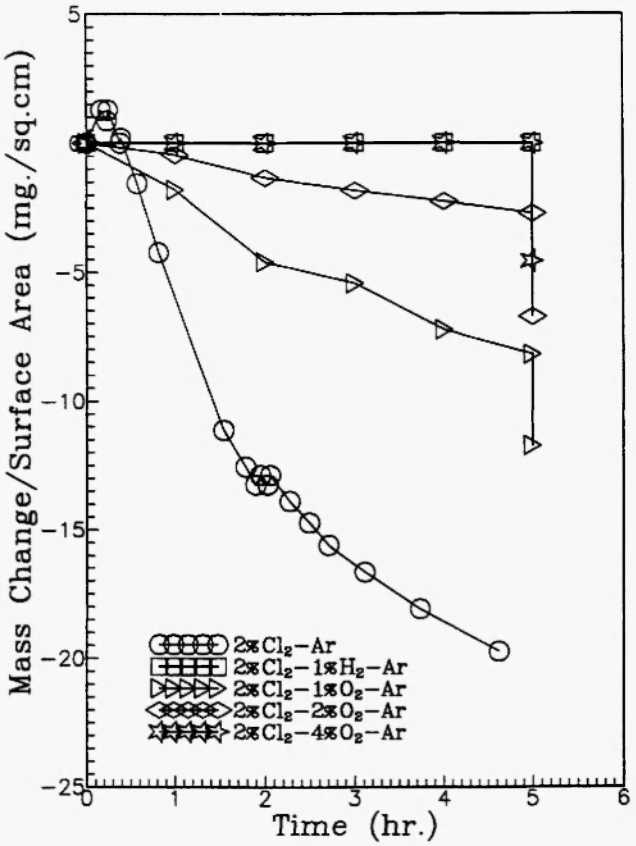

Fig. 9: Thermogravimetric data for CS101K in Ar-2%Cl_2O_2 gas mixtures flowing at 1.5 cm/s at 1000°C.

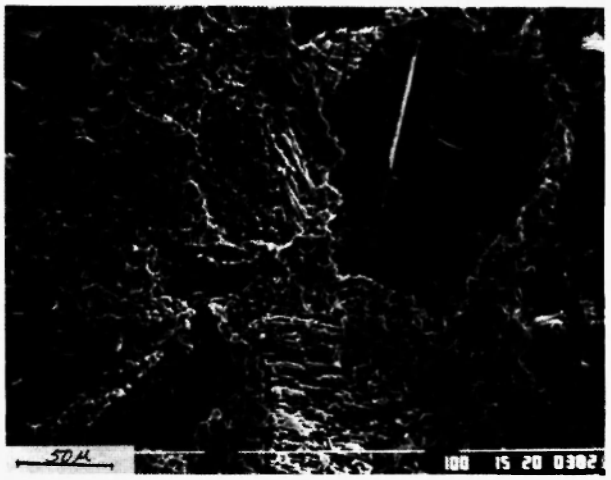

Fig. 10: Scanning electron micrograph of CS101K after corrosion in Ar-2%Cl_2 at 1000°C showing selective attack of free silicon phase and porous SiO_2 deposits.

material experiences active attack in gas mixtures containing higher concentrations of oxygen than the other ceramics. C-600 contains aluminum oxide as a sintering aid. When this material is attacked by chlorine, the oxygen in the sintering aid can contribute to the removal of carbon from the corroding surface. As a result, it is attacked at a higher rate in Ar-2%Cl_2 than the other ceramics. Because of the oxygen contained in the uncorroded material, passive behavior is produced by smaller additions of oxygen to the gas mixture than for the other ceramics. The formation of a passive film may also be favored by the presence of alumina residues on the surface which hinder access to the surface and may react with the silica to form faster growing aluminosilicates. Both SCRB205 and CS101K are siliconized silicon carbides which contain excess silicon rather than carbon. Because the silicon does not contain carbon, it can be attacked more rapidly in low oxygen environments than SiC leading to selective attack of this phase. It is to be noted that all of these materials form passive films in gas mixtures with sufficiently high oxygen levels (20%) /14/.

All of the materials also experienced low rates of corrosion in gas mixtures consisting of Ar-2%Cl_2-1%H_2. From the standpoint of the thermodynamics of SiO_2 formation, the Ar-2%Cl_2 gas mixture still contains sufficient oxygen for this phase to be stable, since technical grades of chlorine typically contain O_2 contamination at levels on the order of 10^{-4} atm. The addition of H_2 to the mixture was intended to tie up the oxygen as H_2O and produce a lower effective oxygen pressure. The amount of the hydrogen addition was kept low compared with the amount of chlorine in the atmosphere, so that HCl formation would not significantly lower the chlorine potential. If the gas mixture comes to thermodynamic equilibrium, however, virtually all of the hydrogen will be converted to HCl, and the effect on the oxygen potential will also be small. As a result, it is not entirely clear why the addition of hydrogen to the gas mixture inhibits the attack. If the oxygen pressure in the corroding gas mixture is low enough that graphite is thermodynamically stable, then a protective film of graphite may form on the surfaces, because the thermodynamic stability of $CCl_4(g)$ is substantially lower than that of $SiCl_4(g)$ at these temperatures.

Temperature also influences the active to passive transition. Figure 11 shows the thermogravimetric data for SASC in Ar-2%Cl_2-2%O_2 at 1100°C. This gas composition produced the highest rates of attack of SASC at 1000°C, and the rates of attack of this material were shown to be controlled by mass transfer in the gas phase. At 1100°C, the rates of attack were substantially smaller than at 1000°C, and there was no consistent effect of gas flow rate on the rate of attack, indicating that mass transfer in the gas phase was no longer rate controlling. Substantial amounts of porous SiO_2 corrosion products were formed on this material during the attack as shown by the weight losses after etching in HF indicated by the vertical dashed lines at the ends of the experiments.

Examination of the specimens tested at 1100° after corrosion showed that this change in behavior was due to localized regions of active corrosion on specimens which were otherwise passive. Figure 12 shows the

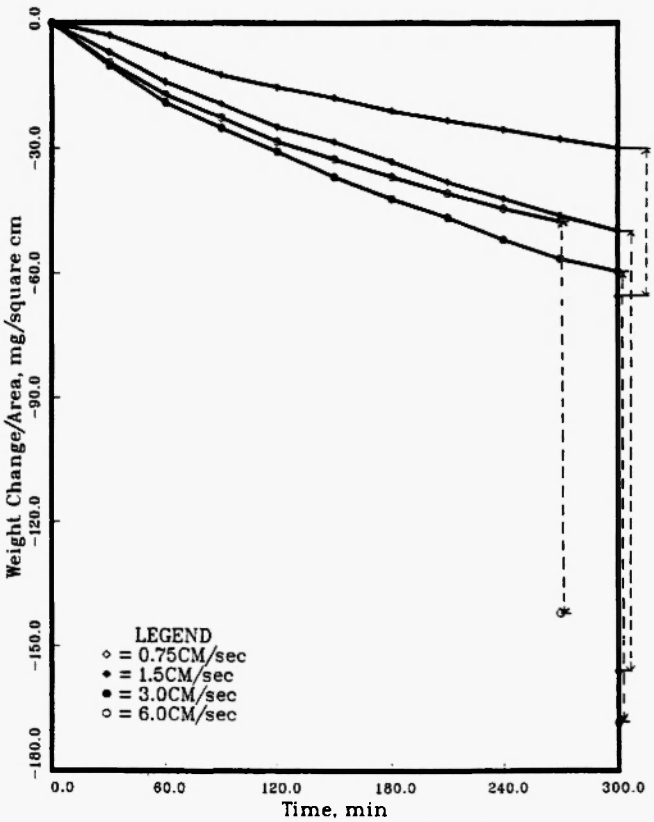

Fig. 11: Thermogravimetric data for SASC in Ar-2%Cl_2-2%O_2 at 1100°C as a function of gas flow rate.

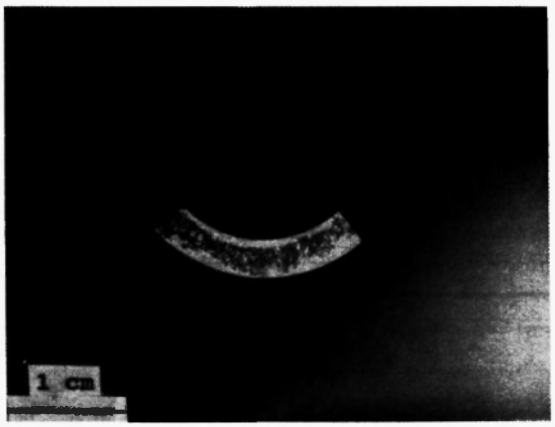

Fig. 12: Photograph of SASC specimen after corrosion in Ar-2%Cl_2-2%O_2 flowing at 3 cm/s at 1100°C.

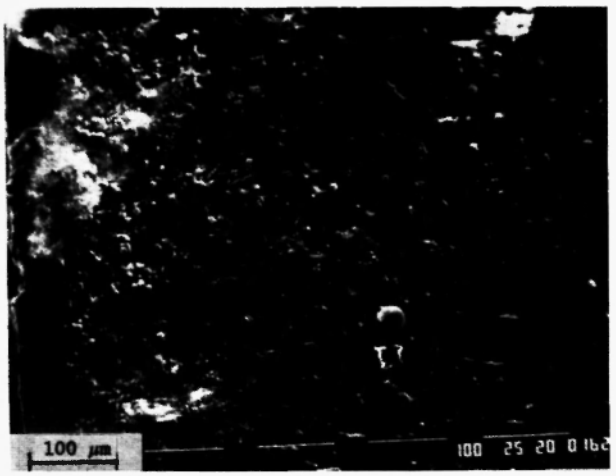

Fig. 13: Scanning electron micrograph of SASC specimen after corrosion in Ar-2%Cl_2-2%O_2 gas mixture flowing at 6 cm/s at 1100°C.

appearance of the specimen tested at a gas flow rate of 3 cm/s after the corrosion. The white areas around the edges of the specimen are porous SiO_2 oxidation products. Figure 13 is a scanning electron micrograph of the surface of the specimen tested at a gas flow rate of 6 cm/s after corrosion, showing a region which includes both porous corrosion products and the darker surface of the ceramic nearby. The appearance of the darker ceramic is very similar to that of the uncorroded

material. Figure 14 shows the same surface after etching in HF to remove the porous oxidation products. Deep pits have formed in the regions where the porous oxidation products had been. This indicates that active corrosion had proceeded in some regions of the specimen while most of the surface was covered by a passive SiO_2 film. Because active corrosion only occurred on some parts of the surface at 1100°C, the overall rate of attack was lower than at 1000°C. It is known that this type of SiC contains local regions where the carbon and boron concentrations are enriched in comparison to the average, and these regions can be sites for accelerated corrosion by molten salts /15-17/. These regions may also be sites for increased susceptibility to active corrosion in oxygen-chlorine mixtures.

E. Silicon Nitride and Nitride Bonded Silicon Carbide

Because of the stability and protective properties of silicon oxynitride, silicon nitride is more resistant to oxidation than silicon carbide /18-20/. Non oxide ceramics produced by chemical vapor deposition can be fabricated without the sintering aids and other impurities found in engineering ceramics and, therefore, experiments were performed on CVD materials to investigate the differences between the corrosion rates of silicon carbide and silicon nitride in chlorine containing environments. Figure 15 shows the thermogravimetric results obtained for CVD SiC, CVD Si_3N_4, and a commercial sintered silicon nitride (GTE AY6, with alumina and yttria sintering aids) in Ar-2%Cl_2 at 1000°C, an environment that produced rapid active attack in all of the engineering silicon carbide ceramics. The CVD SiC is attacked rapidly as were the engineering SiC based ceramics. Neither the CVD silicon nitride nor the engineering silicon nitride material was subject to active corrosion in this environment, indicating that the resistance to attack is generic to the Si_3N_4 based materials /21/.

Nitride bonded silicon carbides are relatively low cost composites of silicon carbide and silicon nitride which are produced by sintering SiC with excess Si in a nitriding environment. A network of reaction bonded silicon nitride forms between the SiC grains to produce a strong composite material. Such composites may provide a good combination of the corrosion resistance of silicon nitride with the excellent physical and

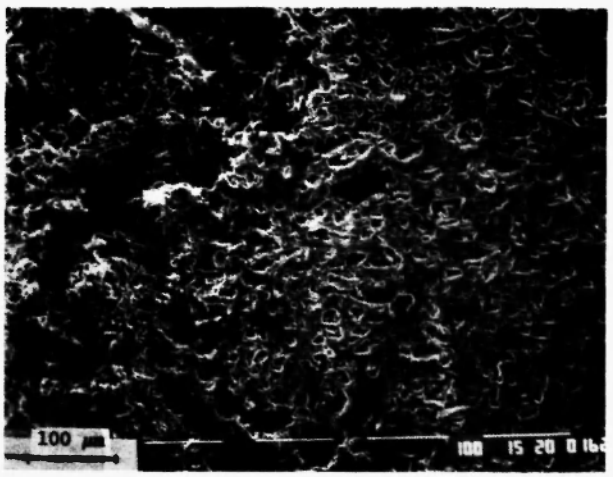

Fig. 14: Scanning electron micrograph of SASC specimen after corrosion in Ar-2%Cl_2-2%O_2 gas mixture flowing at 6 cm/s at 1100°C and etching in HF to remove porous SiO_2 corrosion products and reveal localized corrosion.

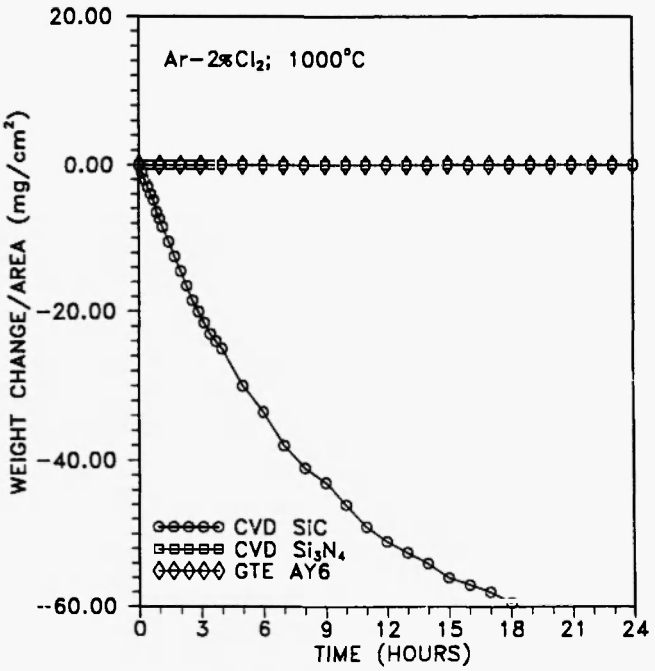

Fig. 15: Thermogravimetric data for CVD SiC, CVD Si_3N_4, and GTE AY6 silicon nitride based ceramic in Ar-2%Cl_2 at 1000°C.

mechanical properties of silicon carbide. Reaction formed silicon nitride is porous, however, and the SiC grains in this material may be susceptible to attack by chlorine in corrosive gas mixtures. A series of tests were performed on nitride bonded SiC ceramics in Ar-2%Cl_2-O_2 gas mixtures to investigate the resistance of these composites to active attack in Cl_2-O_2 gas mixtures.

Figure 16 shows thermogravimetric results for a nitride bonded SiC material tested at 900°C in the same series of environments as shown for SiC in Figures 6-9. The results are similar to those for the siliconized SiC materials tested in the same environments. The highest corrosion rates are produced in Ar-2%Cl_2 and all additions of oxygen to the environment reduce the rate of attack. Little or no attack is produced in Ar-2%Cl_2-20%O_2, where a passive film on the SiC is to be expected or in Ar-2%Cl_2-1%H_2 where the hydrogen inhibits the active attack.

Figure 17 shows thermogravimetric results for a similar material with finer SiC grains exposed at

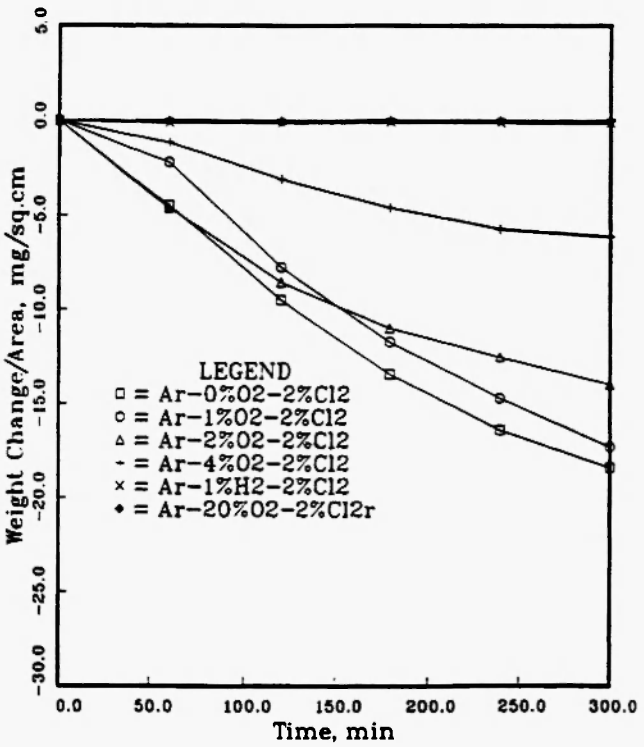

Fig. 16: Thermogravimetric data for nitride bonded SiC in gas mixtures containing 2%Cl_2 at 900°C.

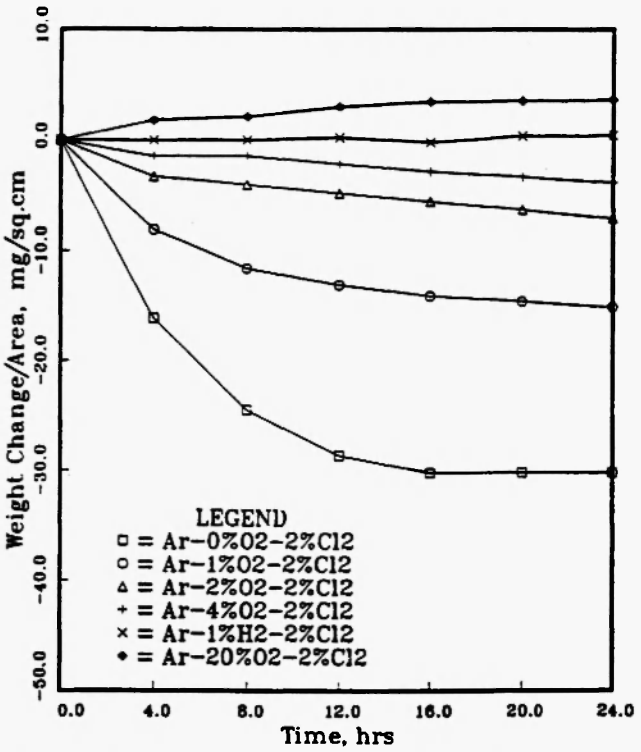

Fig. 17: Thermogravimetric data for nitride bonded SiC with fine SiC particle size in gas mixtures containing 2%Cl_2 at 1000°C.

1000°C. Although the general features of the corrosion behavior are similar, there are two significant differences. There is a measurable increase in the mass of the specimen after exposure to Ar-2%Cl_2-20%O_2 where a passive silica film is expected to form. This is likely to be the result of the higher surface to volume ratio of the fine SiC particles in this material, such that the formation of the SiO_2 film on this area produces a larger increase in mass than the formation of a film of the same thickness over the surface area of a dense ceramic. The second difference is that the mass of the specimen exposed to Ar-2%Cl_2 decays to a minimum value after approximately 14 hours of exposure. This can be related to the selective attack of the SiC phase within the composite.

Figure 18 shows scanning electron micrographs of a nitride bonded SiC material in the as cut state and after exposure to Ar-2%Cl_2-2%O_2 at 1000°C for 24 hours. It is clear that the corrosion has been selective for the SiC grains which have receded within the Si_3N_4 matrix after the exposure. Examination of the specimens

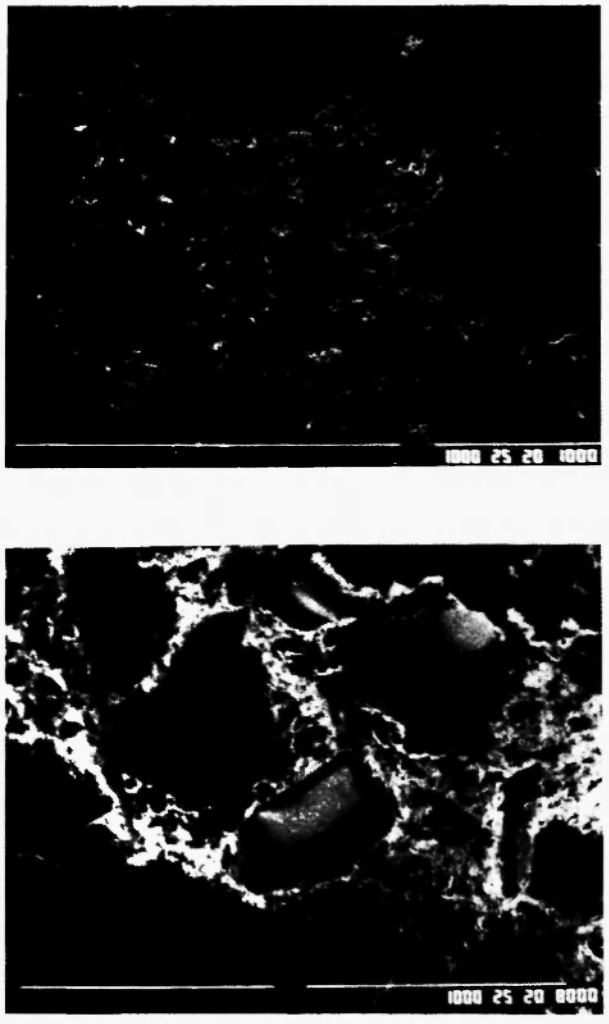

Fig. 18: Scanning electron micrographs of nitride bonded SiC materials in as-cut state (a) and after exposure to Ar-2%Cl_2-2%O_2 at 1000°C (b).

which had been corroded to the minimum mass state in Ar-2%Cl_2 revealed only porosity in the locations where the SiC grains had been. X-ray diffraction analysis of the specimen after corrosion detected only silicon nitride and silicon oxynitride. Examination using EDS microanalysis with a light element detector showed that the material contained only silicon, oxygen and nitrogen, indicating that the SiC had been completely consumed and that the remaining specimen consisted only of silicon nitride, silicon oxynitride and silicon oxide /22/.

The rate of active corrosion of the SiC grains was controlled by temperature and the surface to volume ratio of the grains. Figure 19 shows the relative weight loss of the same nitride bonded silicon carbide from Figure 16 exposed to Ar-2%Cl_2 and plotted as a fraction of the initial mass of the specimen at temperatures from 900 to 1200°C. The rate of attack increases with increasing temperature with the mass decaying to a consistent minimum value in 24 hours at 1000°C, 12 hours at 1100°C, and 6 hours at 1200°C. Figure 20 shows the relative weight losses of three types of nitride bonded SiC materials exposed to Ar-2%Cl_2 at 1000°C. The rate of attack of the materials increases as the particle size of the SiC grains in the material decreases. This is consistent with a model in which the corrosion reaction occurs over the surface of the SiC grains and the overall rate of attack is proportional to the specific surface area of the SiC. Other experiments indicated that mass transport through the pores in the Si_3N_4 skeleton may influence the rate of corrosion for thicker specimens than those used in these tests /22/.

F. Summary

Active corrosion of SiC based ceramics can occur in

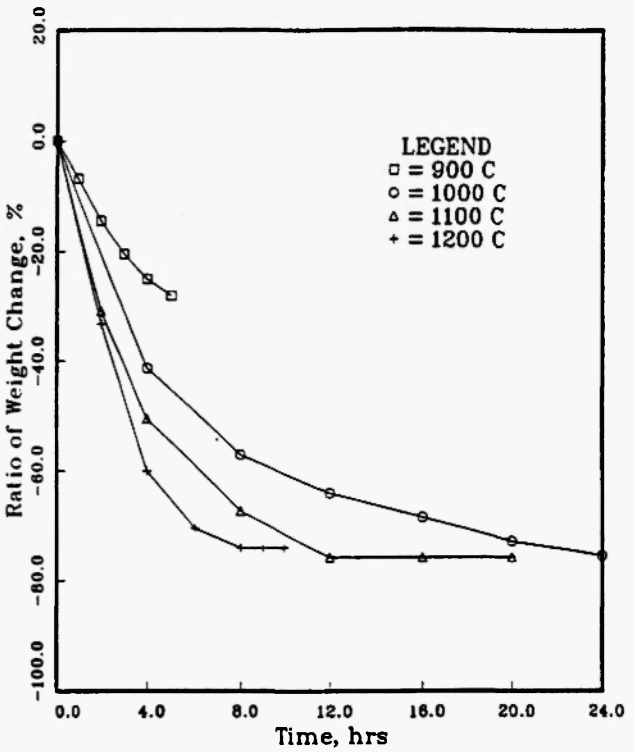

Fig. 19: Relative mass loss of nitride bonded SiC material with fine grain size in Ar-2%Cl_2 at temperatures between 900 and 1200°C.

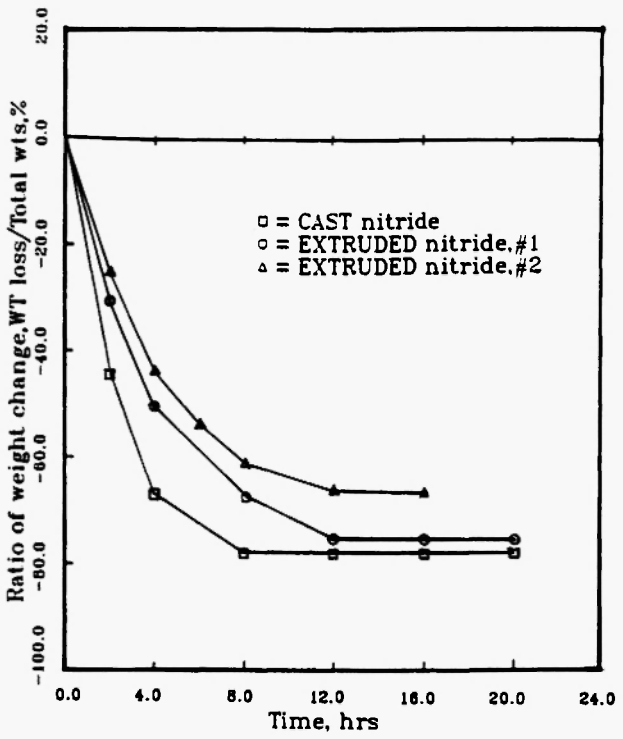

Fig. 20: Relative mass loss of nitride bonded SiC materials with different SiC particle sizes in Ar-2%Cl_2 at 1000°C.

gas mixtures containing high concentrations of chlorine at temperatures above 900°C. Corrosion by this mechanism obeys a linear rate equation and is several orders of magnitude faster than oxidation in clean air. Formation of a passive SiO_2 film can inhibit this form of attack in mixed oxygen-chlorine gases if the ratio of oxygen to chlorine in the gas mixture is high enough. If the ratio of oxygen to chlorine is not high enough to form a passive film, active corrosion can occur with simultaneous formation of volatile $SiCl_4$ and SiO_2 with a porous non-protective morphology. Reducing chlorine containing mixtures containing hydrogen do not produce active attack at temperatures up to 1000°C.

In a gas mixture with a fixed oxygen to chlorine ratio, both the corrosion rate and the tendency toward formation of a passive film is favored by raising the temperature of the exposure so that corrosion rates may increase or decrease with increasing temperature. Engineering SiC based ceramics containing boron or excess carbon as sintering aids experience active corrosion in gases with higher oxygen contents than other SiC based ceramics. SiC ceramics with aluminum oxide as a sintering aid experience faster attack in environments with low oxygen potentials, but passivate more easily in comparison to other SiC materials. Siliconized silicon carbides are subject to selective attack of the free silicon phase by active corrosion. Silicon nitride is much more resistant to active corrosion than silicon carbide. SiC grains in nitride bonded SiC are selectively attacked in chlorine containing environments leaving behind a porous framework of silicon nitride.

III. DISRUPTION OF THE SiO_2 PASSIVE FILM

A. Introduction

Even under conditions where a passive silica film is formed, chlorine additions can produce accelerated oxidation by disrupting the orderly growth of the silica layer at high temperatures. Experiments to investigate this phenomenon were performed using the apparatus shown schematically in Figure 1.

B. Results and Discussion

Figure 21 shows thermogravimetric results for oxidation of SASC at 1300°C in Ar-2%Cl_2-20%O_2. Under these conditions the specimen experiences a net increase in mass due to the growth of condensed oxide corrosion products, but the rate of this mass increase is higher than would be expected in uncontaminated oxygen. The reason for the increased corrosion rate can be inferred from examination of the surface of the specimen after corrosion. The surface is covered by a number of large bubbles as shown in Figure 22. These bubbles apparently form due to the penetration of chlorine through the dense SiO_2 film to the region of low oxygen potential near the SiC/SiO_2 interface where volatile compounds such as $SiCl_4$ are formed. Because $SiCl_4$ molecules are larger than Cl_2, they may not be able to dissolve in the silica network and diffuse back out, and therefore cause bubble growth in the scale. Similar formation of chlorine rich phases and bubbles near the SiO_2/Si interface has been observed during oxidation of silicon in O_2/HCl ambients and during

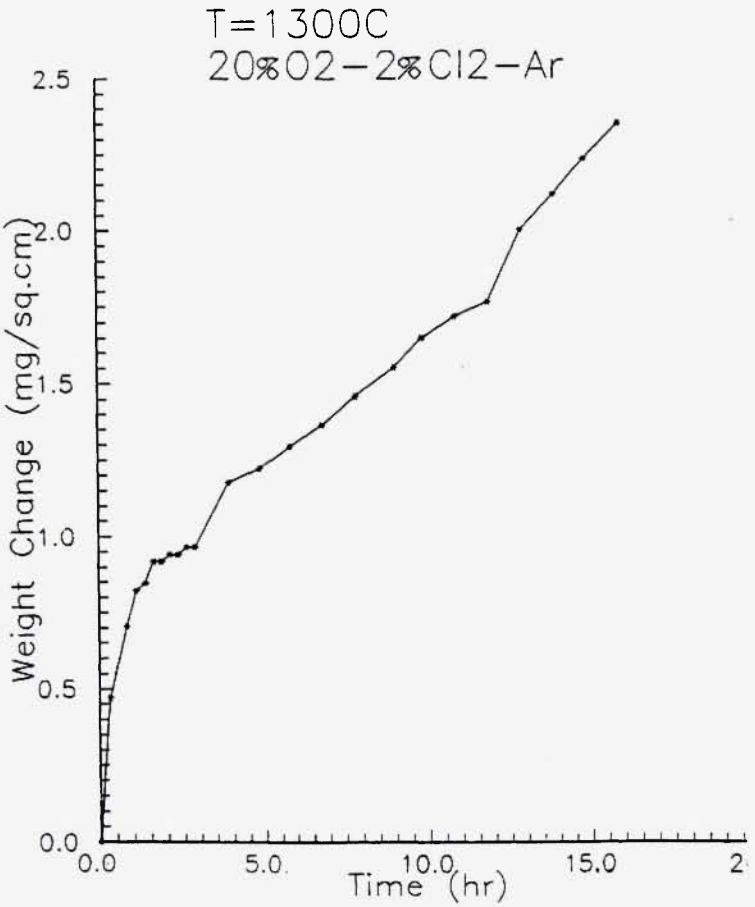

Fig. 21: Thermogravimetric results for oxidation of SASC in Ar-2%Cl_2-20%O_2 at 1300°C.

Fig. 22: Photograph of SASC specimen after oxidation in Ar-2%Cl_2-20%O_2 at 1300°C.

oxidation of single crystal SiC in O_2/Cl_2 mixtures /23-25/.

Bubble formation in the silica film was also observed at lower temperatures and for other SiC based ceramics as shown in Figure 23. At lower temperatures, the bubbles are smaller. At higher temperatures, the size of the bubbles was larger, and ultimately bubbles with diameters up to a centimeter could be formed as shown in Figure 22. The growth of the bubbles can increase the corrosion rate by stretching the silica film and reducing the distance that dissolved oxygen must be transported before it can react with the underlying ceramic. Because the bubbles formed at 1300°C were large enough to be observed without the use of electron microscopy, the apparatus shown schematically in Figure 1 was modified to permit the sample to be viewed through the bottom of the reaction tube during corrosion, and a series of simultaneous TGA/bubble growth experiments were performed.

Figure 24 shows bubble formation on the SCRB210 sample during oxidation in Ar-2%Cl_2-20%O_2 at 1300°C. Bubbles begin to form on the sample after approximately 1 hour of exposure to the environment. Once bubble formation has begun, the kinetics of the attack follow a linear rather than a parabolic rate equation. It is likely that transport through the film is still rate controlling for the oxidation, but continuous disruption of the film prevents it from providing an increasingly effective diffusion barrier as would be expected in uncontaminated oxygen. Large bubbles

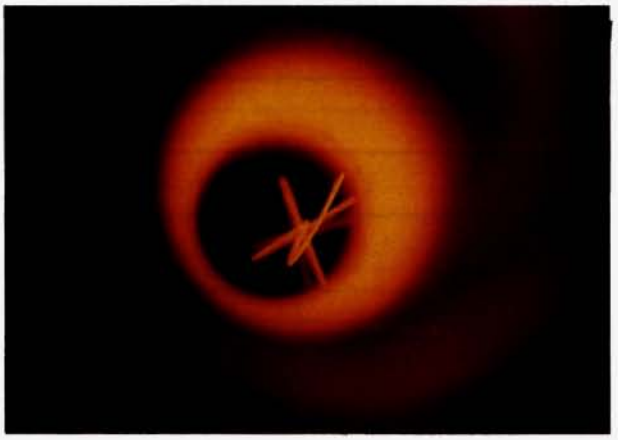

Fig. 24: Photographs of *in situ* bubble formation in SiO_2 film on SCRB 210 in Ar-2%Cl_2-20%O_2 at 1300°C.

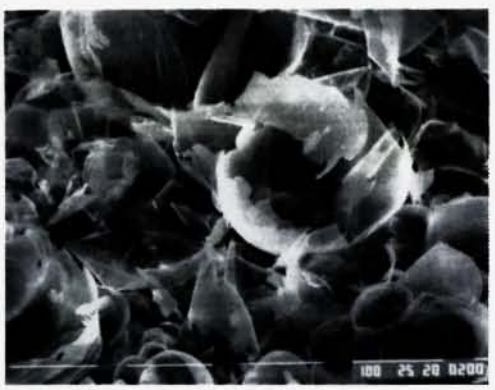

Fig. 23: Scanning electron micrograph of bubbles in SiO_2 film on SASC formed during oxidation in Ar-2%Cl_2-20%O_2 at 1100°C.

continuously nucleate, grow, coalesce, and burst during the course of the experiment. In this experiment, the bubbles grew large enough to contact the wall of the reaction tube after approximately 7 hours of oxidation.

Similar experiments were performed with SASC and C-600 material. Figure 25 shows an example of the bubbles formed on SCRB 210. Scanning electron microscopy on siliconized silicon carbide specimens exposed at lower temperatures showed that the interfaces between the SiC grains and the free silicon phase served as nucleation sites for bubble formation. Because there were many such nucleation sites on the surfaces of the siliconized silicon carbide, a large number of small bubbles formed on the surface of the

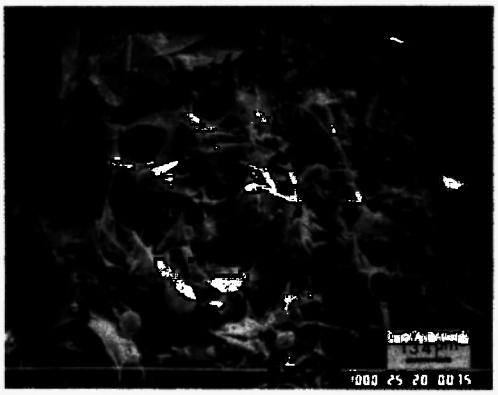

Fig. 25: Scanning electron micrograph of bubbles in SiO_2 film on SCRB 210 showing foam of fine bubbles nucleated at Si/SiC interfaces.

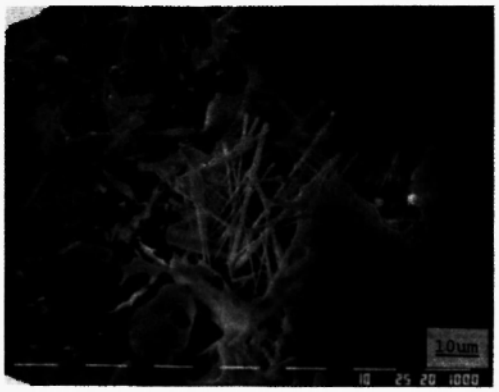

Fig. 26: Scanning electron micrograph of bubble and aluminum containing crystalline phase formed on C-600 during oxidation in Ar-2%Cl_2-20%O_2 at 1300°C.

SCRB 205 producing a foam in which individual bubbles could not be easily resolved in the *in situ* experiments. The effect was similar for SASC except that a smaller number of large bubbles grew from a smaller number of nucleation sites.

A few small bubbles were observed on the C-600 surfaces at the beginning of the experiment, but these burst quickly and no further bubble formation was found on this material. The reason for this behavior was found by examination of the exposed surfaces by scanning electron microscopy. Figure 26 shows a micrograph of a bubble on the C-600 surface after exposure. The bubble is penetrated by needles of a phase which EDS microanalysis showed was rich in aluminum. The alumina sintering aid in the C-600 reacted with the amorphous silica film on the surface to form crystalline reaction products (probably mullite). This phase did not have the capacity for plastic deformation necessary to produce bubbles, and therefore, the bubbles burst and accelerated oxidation stopped after this reaction.

Similar bubble formation was observed on CVD SiC specimens oxidized in Ar-2%Cl_2-20%O_2 at 1300°C as shown in Figure 27, and the bubble formation was associated with a similar increase in the oxidation rate in comparison to the rate in uhcontaminated oxygen. The bubbles formed on the CVD material at 1300°C were smaller than those on the engineering ceramics at the same temperature. When CVD Si_3N_4 was exposed to the same environment, no bubble formation was observed as shown in Figure 28. This is consistent with the superior resistance of silicon nitride to active corrosion in chlorine-oxygen mixtures. No bubble formation or accelerated oxidation was observed for engineering silicon nitride materials in the same environment /21/.

Nitride bonded silicon carbide ceramics were also tested in Ar-2%Cl_2-20%O_2 at 1300°C and also exhibited accelerated oxidation and paralinear kinetics as shown in Figure 29. Bubble formation in the silica films on these specimens was found to initiate on the SiC grains in the ceramics and not in the Si_3N_4 matrix. This is shown in Figure 30. This is similar to the

Fig. 27: Scanning electron micrograph of bubbles formed on CVD SiC oxidized in Ar-2%Cl_2-20%O_2 at 1300°C.

Fig. 28: Scanning electron micrograph of surface of CVD Si_3N_4 after exposure to Ar-2%Cl_2-20%O_2 showing that no bubbles were formed.

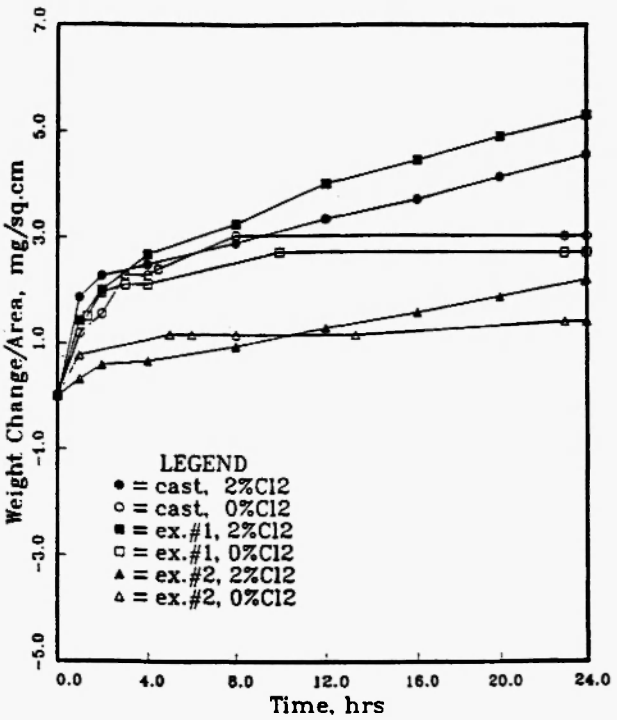

Fig. 29: Thermogravimetric results for nitride bonded SiC materials in Ar-2%Cl_2-20%O_2 at 1300°C showing accelerated oxidation in comparison to results in Ar-20%O_2.

behavior of these materials in the environments which produced active corrosion, in that the overall corrosion behavior of the composite is dominated by the

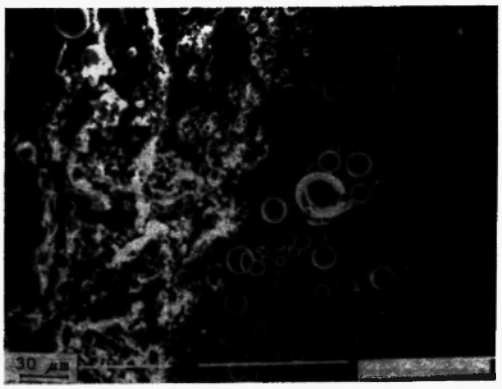

Fig. 30: Scanning electron micrograph of oxidized surface of nitride bonded SiC material showing bubble formation on SiC grains.

performance of the SiC phase which is attacked by gases diffusing through the porous Si_3N_4 /22/.

Bubble formation was also observed on specimens which were corroded at 1300°C in gas mixtures containing as little as 0.5%Cl_2 and as little as 2%O_2. Gas mixtures which contained 0.1%Cl_2 did not produce bubble formation but still exhibited accelerated oxidation in comparison to the rate produced in uncontaminated oxygen. Gas mixtures containing Cl_2 without oxygen additions at 1300°C produced active corrosion. Preoxidation of the ceramics in clean oxygen before introduction of chlorine delayed the formation of bubbles but did not prevent accelerated attack or alter the final morphology of the corrosion products. Single crystal silicon also oxidizes with bubble formation in Ar-2%Cl_2-20%O_2 at 1300°C /21/.

C. Summary

In summary, the accelerated oxidation produced by chlorine during passive oxidation at temperatures up to 1300°C appears to occur primarily by the penetration of chlorine through the SiO_2 film to form volatile silicon chloride products at the SiC/SiO_2 interface. The growth of the bubbles disrupts and thins the protective film and reduces its capability to separate the ceramic from the environment. The chlorine may also act as a network modifier in the SiO_2 structure reducing its viscosity and increasing its permeability to oxygen. SiO_2 in uncontaminated oxygen would not be expected to have

sufficient plasticity to form large bubbles at 1300°C and some accelerated oxidation was observed in environments containing 0.1%Cl_2 where bubble formation was not observed. Silicon nitride was resistant to this form of attack. Nitride bonded silicon carbides were subject to selective attack of the SiC phase by gases penetrating through the porous Si_3N_4. Engineering silicon carbides containing alumina as a sintering aid were more resistant to this attack than other engineering silicon carbides because the alumina sintering aids reacted with the SiO_2 oxidation products to devitrify the film and prevent bubble formation. In general, the rates of attack produced by this mechanism were much lower than those produced by active attack, so these considerations may be less serious than those which affect the active to passive transition.

IV. CORROSION IN ALKALI HALIDE VAPORS

A. Introduction

In many industrial applications the halogen specie is likely to be present in the environment as an alkali halide. This includes aluminum remelting furnaces where sodium and potassium chlorides are used as a flux to protect the metal from oxidation /26/. Molten alkali chloride deposits on a ceramic surface can produce hot corrosion of silicon based ceramics by mechanisms which have been reviewed elsewhere /27/. Alkali species are effective in causing accelerated oxidation of both SiC and Si_3N_4 /28,29/. Because of their high volatility in comparison to other salts, alkali halides can be present in sufficient quantities to cause accelerated attack even when they are present only in the vapor phase. The attack produced by these species is distinct from that produced in elemental halogens alone in that the alkali rather than the halogen is the most important corrosive agent.

B. Apparatus and Procedures

The apparatus used to investigate corrosion in the presence of alkali chloride vapors is shown schematically in Figure 31. It consists of two furnaces connected in series. A gas mixing and purification system similar to that shown in Figure 1 is used to purify and blend reagent gases which are supplied to the water saturator on the right hand side of the figure. The gases then flow downward through an alumina tube into a molten salt bath in the lower furnace. The temperature of the lower furnace fixes the vapor pressure of the salt vapor in the corrosive gas mixture which flows upwards through the furnace. The calculated vapor pressures were checked by comparison with the mass changes of the salt bath. Table II shows the agreement between the calculated and measured vapor pressures.

The samples to be tested were suspended from an alumina rack in the center of the upper furnace. The upper furnace was always maintained at a higher temperature than the lower furnace to avoid condensation of liquid chlorides on the samples. The gases exited through a firebrick or metal cap at the top of the furnace. Condensation of solid salt crystals at this location limited the duration of some of the experiments with high vapor pressures of alkali chlorides.

The experiments were initiated by suspending the specimens in the furnace, bringing the furnace to

Table 2
The Comparison of the Vapor Pressure of Salt

Salt	Salt temperature	Experimental vapor pressure	Calculated vapor pressure
NaCl	874°C	1.14×10^{-3} atm.	0.81×10^{-3} atm.
NaCl	836°C	5.07×10^{-4} atm.	4.10×10^{-4} atm.
NaCl	815°C	4.58×10^{-4} atm.	2.94×10^{-4} atm.
KCl	790°C	7.43×10^{-4} atm.	5.05×10^{-4} atm.
KCl	837°C	1.18×10^{-3} atm.	1.19×10^{-3} atm.

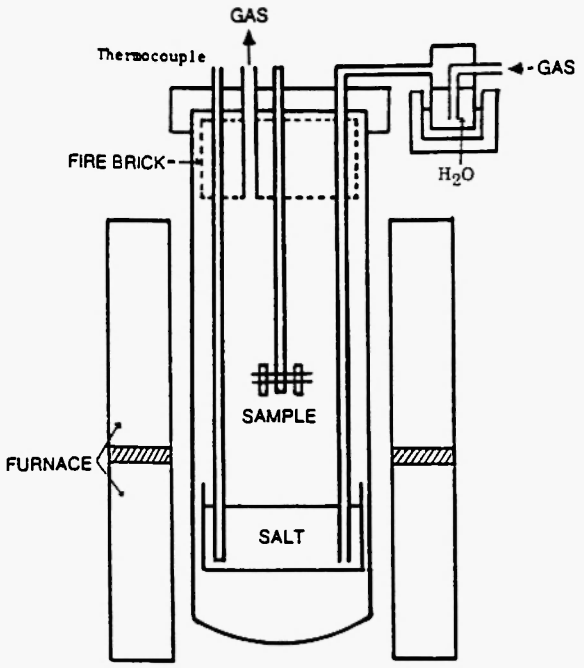

Fig. 31: Schematic diagram of apparatus used for experiments in alkali chloride containing environments.

temperature in stagnant air, and then initiating the flow of the corrosive gases. At the conclusion of the experiments, the samples were removed from the furnace and evaluated by scanning electron microscopy and measurement of the change in mass. The quantity of alkali silicates and SiO_2 on the surface was evaluated by measuring the mass changes after sequential etching in hot water and HF using a method originally described by Jacobson *et al.* /30,31/.

C. Results and Discussion

Figure 32 shows typical results for corrosion of SASC in Ar-20%O_2-0.105%KCl(g) at 900°C. This gas mixture was produced by passing a dry mixture of Ar-20%O_2 through the system with the bottom zone of the furnace maintained at 850°C. The results of three separate experiments of 25, 50 and 75 hours duration are shown. The specimen experiences attack at an approximately linear rate in this environment. Figure 33 shows a scanning electron micrograph of an SASC specimen after corrosion. Little chlorine is detected by EDS on the surface, but a substantial amount of potassium is present, indicating that the layer is potassium silicate. When the potassium silicate is removed by soaking in hot water, the specimen experiences a linear decrease in mass due to corrosion as shown in Figure 32. Further etching in HF produced very little change in mass, indicating that the pure SiO_2 layer expected between the silicate and the SiC was thin or non-existent in this environment.

The linear corrosion kinetics observed in Figure 32 are to be expected because potassium silicate is liquid at 900°C and would not provide a protective layer for the SiC. Under these conditions the critical step in the corrosion process is expected to be the fluxing of the protective SiO_2 layer to form the alkali silicate. This reaction can be written for the disilicate:

$$2KCl\,(g) + 0.5O_2\,(g) + 2SiO_2\,(s) = K_2Si_2O_5\,(l) + Cl_2\,(g) \quad (1)$$
$$G° = 61{,}127\ J/mol\ at\ 900°C$$

By this mechanism, it is the potassium, rather than the chlorine, that is the principal corrosive agent and the chlorine is important only because the potassium chloride has a high enough vapor pressure to transport large amounts of the alkali metal to the oxidizing surface. Although the Gibbs free energy change of

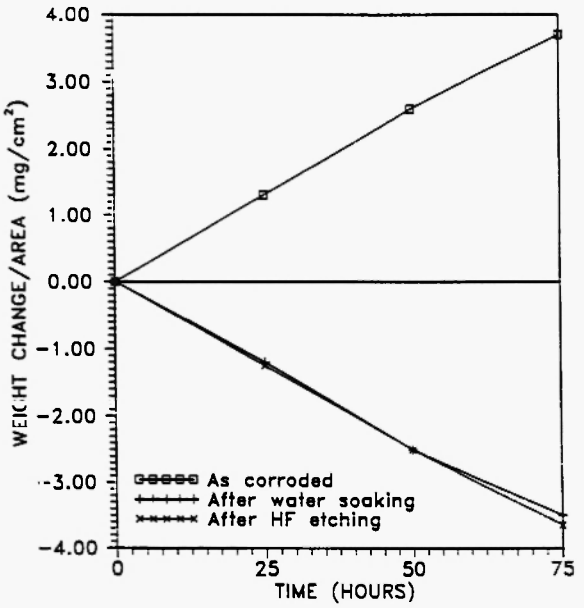

Fig. 32: Thermogravimetric results for SASC in Ar-20%O_2-0.105%KCl (g) at 900°C.

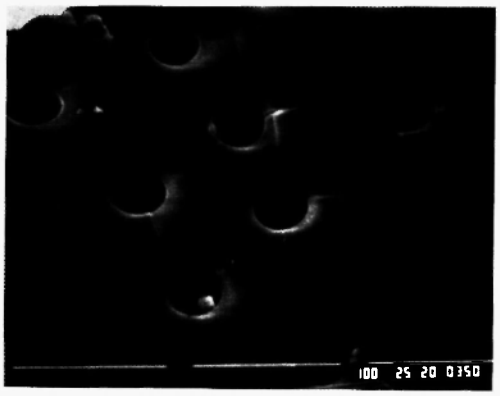

Fig. 33: Scanning electron micrograph of SASC specimen after corrosion in Ar-20%O_2-0.105%KCl at 900°C.

reaction (1) is positive, a liquid product having a potassium to silicon ratio of less than 1 to 2 and a low activity of K_2O could still form. Furthermore, the activity of the potassium as an oxide species in the silicate is a more complex property than the partial pressure of the alkali chloride alone. It is influenced by temperature and by the partial pressures of the other species (O_2 and Cl_2) in the gas phase.

Water vapor can have a large effect on the corrosivity of the alkali chloride, because in the presence of water vapor equation (1) is replaced by equation (2):

$$\begin{aligned} & KCl\ (g) + H_2O\ (g) + 2SiO_2\ (s) \\ = \ & K_2Si2_2O_5\ (l) + 2HCl\ (g) \qquad (2) \\ & G° = 33{,}660\ J/mol\ at\ 900°C \end{aligned}$$

In the presence of water vapor, the chlorine in the alkali salt can be removed as the stable molecule HCl rather than as Cl_2, and this makes the corrosion reaction substantially more thermodynamically favorable. Therefore, equilibrium K_2O activities in gas mixtures which contain water vapor will be higher than those in dry gas mixtures containing the same partial pressure of KCl.

Figure 34 shows the effect of adding 3%H_2O (g) to the gas mixture used in the experiments from Figure 32. The corrosion still obeys an approximately linear rate equation, but the overall rate of attack is accelerated by approximately a factor of four. Again,

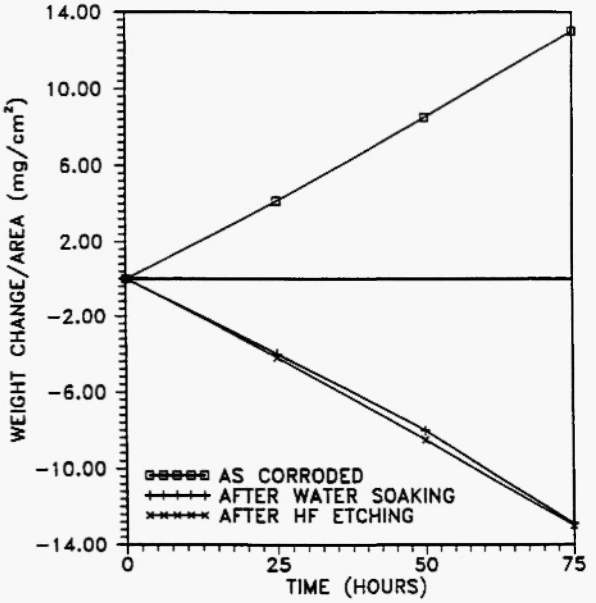

Fig. 34: Thermogravimetric results for SASC in Ar-20%O_2-3%H_2O-0.105%KCl at 900°C demonstrating accelerated corrosion in water vapor containing environment.

little or no SiO_2 layer is detected.

The concentration of KCl in the environment can be varied by changing the temperature of the lower furnace without altering the temperature of the tests in the upper furnace. Figure 35 shows the effect of increasing the partial pressure (or concentration) of KCl on the amount of corrosion of SASC in Ar-20%O_2-3%H_2O in 25 hours at 1000°C. As expected, the amount of attack increases monotonically with increasing partial pressure of KCl. Because the corrosion obeys a linear rate equation, these corrosion amounts are directly related to the corrosion rates. Similar results were obtained for the other engineering SiC ceramics and in NaCl containing gas mixtures as will be discussed later.

The effects of other environmental parameters on the rate of corrosion in KCl containing environment is illustrated in Figure 36 for SASC corroded at 1000°C. For simplicity, only the mass changes after water soaking and etching are shown. The figure shows the changes in mass of specimens after exposure to Ar-20%O_2-0.105%KCl, illustrating a linear decrease in mass at a higher rate than that in Figure 32, which

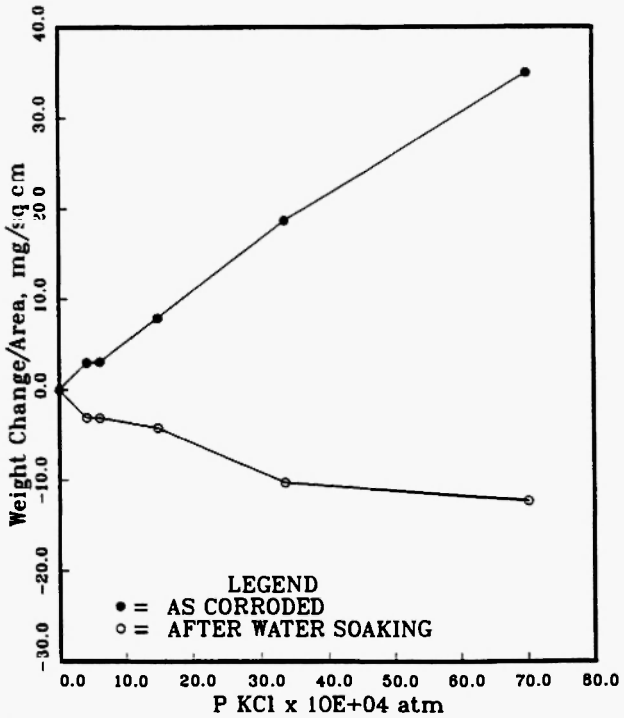

Fig. 35: Effect of KCl pressure on corrosion of SASC in Ar-20%O_2-3%H_2O gas mixtures at 1000°C.

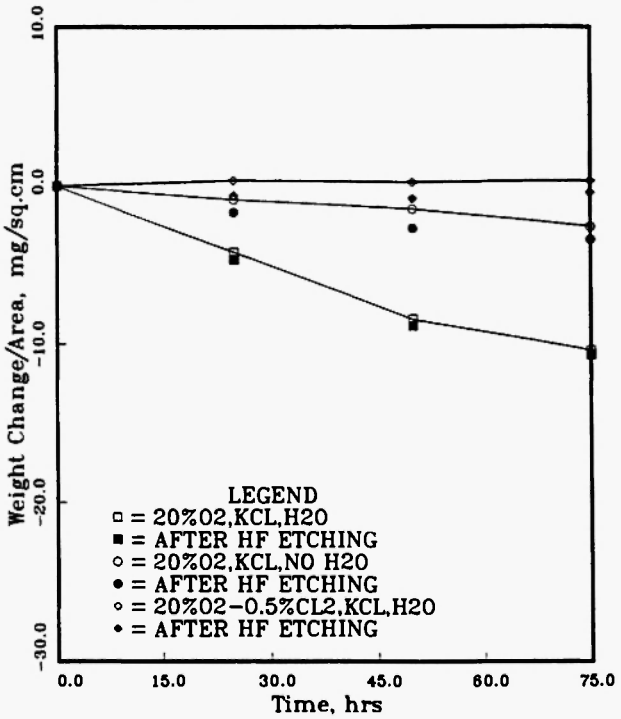

Fig. 36: Mass change results for SASC at 1000°C in Ar-20%O_2-0.105%KCl, Ar-20%O_2-3%H_2O-0.105%KCl, and Ar-20%O_2-3%H_2O-0.5%Cl_2-0.105%KCl showing inhibition of corrosion by chlorine.

indicates that increasing temperature increases the rate of attack. When 3% H_2O is added to the gas mixture, the rate of attack is increased, consistent with the thermodynamics and with the results at 900°C. Finally, when 0.5%Cl_2 is added to the gas mixture, the rate of attack is reduced nearly to zero. This is also consistent with the thermodynamic calculations. Because the alkali rather than the chlorine is the corrosive agent, chlorine additions inhibit, rather than accelerate the attack. By appropriate control of the ratio between alkali chloride pressure and HCl pressure in the environment, the equilibrium activity of the alkali oxide can be calculated and correlated with the corrosion rate /32/.

Similar results are obtained in NaCl containing environments as shown in Figure 37. Because NaCl has lower vapor pressures than KCl, the concentration of NaCl (g) in the atmosphere over molten NaCl is lower than that of KCl over molten KCl at the same temperature. Figure 38 compares the weight change

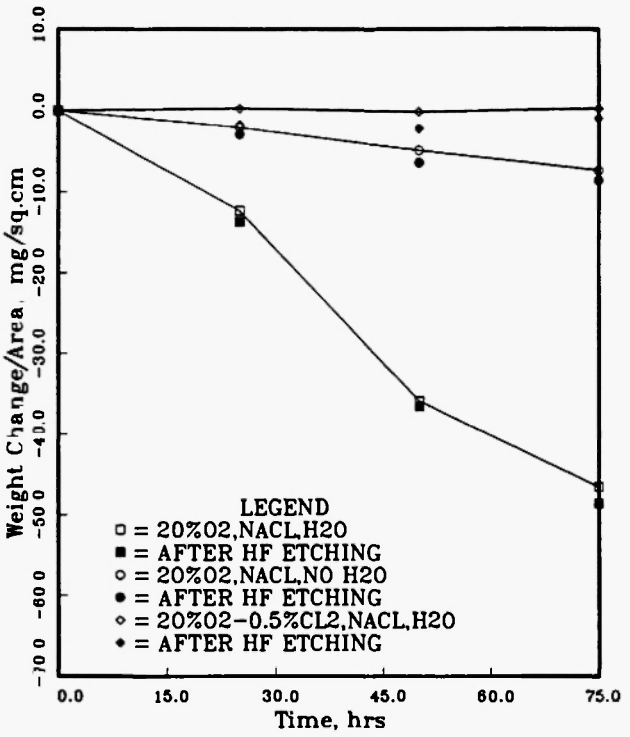

Fig. 37: Weight change results for SASC in Ar-20%O_2-0.05%NaCl (g), dry, with 3% H_2O, and with 3% H_2O and 0.5%Cl_2 showing similar behavior to KCl containing environments.

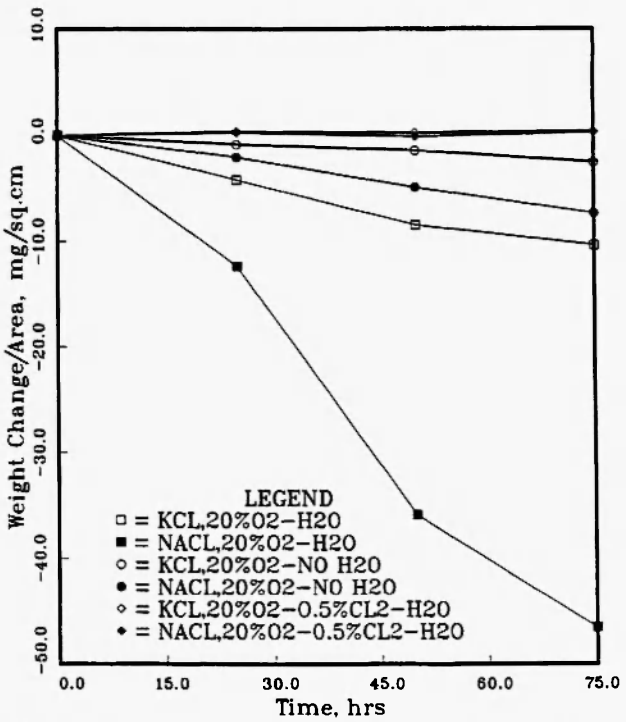

Fig. 38: Comparison of corrosion rates for SASC at 1000°C in Ar-20%O_2-3%H_2O with NaCl or KCl vapors generated at 850°C.

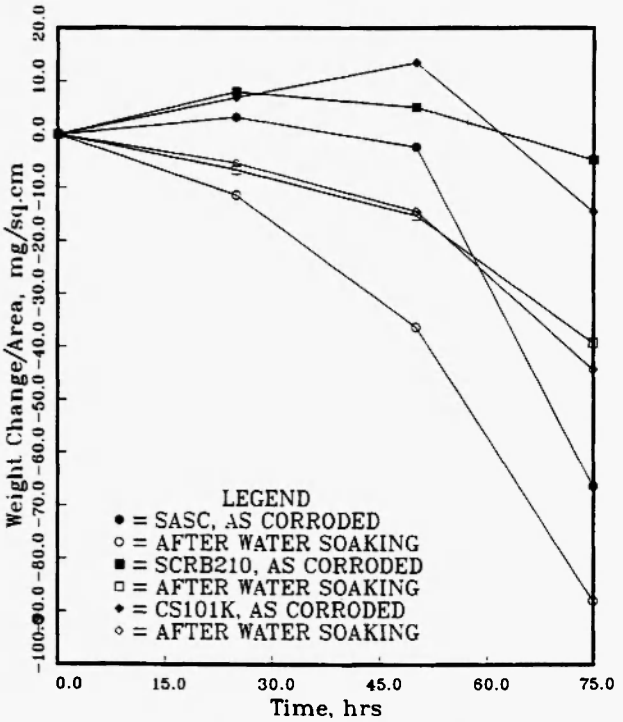

Fig. 39: Weight change results for engineering SiC materials in Ar-20%O_2-3%H_2O-0.105%KCl containing environments at 1100°C showing non-linear kinetics due to flow of corrosion products.

results obtained for SASC at 1000°C in gas mixtures prepared with KCl or NaCl salt melts at 850°C (KCl vapor pressure = 1.05 x 10^{-3} atm, NaCl vapor pressure = 5 x 10^{-4} atm). Although the NaCl vapor pressure is lower, the NaCl containing environment consistently produces higher corrosion rates.

Further increases in the reaction temperature beyond 1000°C produce results which do not fit linear rate equations as shown in Figure 39 for three engineering ceramics exposed at 1100°C to Ar-20%O_2-3%H_2O-0.105%KCl. Weight changes after removal from the furnace and after water soaking are presented. The mass changes after removal from the furnace go through a maximum and decrease again with increasing time. This is because the viscosity of the alkali silicate at this temperature is low enough that the corrosion product layers flow and drip from the surfaces of the specimens during the exposure under these conditions. This fluid flow also accelerates mass transfer in the corrosion product and leads to an increase in the net rate of attack with time, as illustrated by the weight changes after water soaking.

Figure 39 presents results for SASC and two siliconized silicon carbides, SCRB210 and CS101K. The SASC is attacked most rapidly in this environment, possibly because the boron used as a sintering aid in this material further lowers the viscosity of the corrosion product. The two siliconized materials are attacked at approximately the same rate.

Figure 40 shows the surface of an SASC specimen after exposure to Ar-20%O_2-3%H_2O-0.105%KCl at 900°C. The glassy corrosion product is typical of the corrosion products formed in all of the alkali chloride containing environments. EDS microanalysis of this material detected only K and Si. In some experiments a small amount of Cl could be detected, but this could usually be attributed to chlorides deposited on the surface of the corroded sample during cooling and removal from the furnace. Figure 41 shows the surface of the SASC specimen after the corrosion product had been removed by water soaking. The pitted morphology is consistent with the morphology of this material after

Fig. 40: Scanning electron micrograph of surface of SASC specimen after corrosion in Ar-20%O_2-3%H_2O-0.105%KCl environment at 900°C.

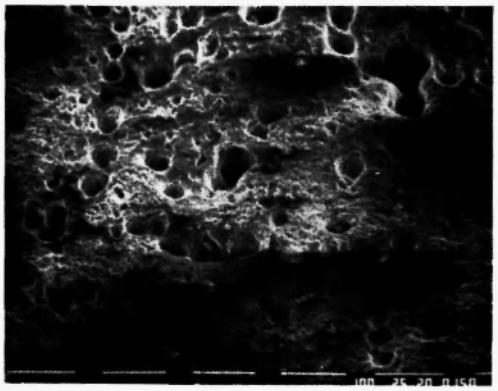

Fig. 41: Scanning electron micrograph of surface of SASC specimen after corrosion in Ar-20%O_2-3%H_2O-0.105%KCl environment at 900°C and etching in hot water to remove corrosion products showing pitted nature of corroded surface.

molten salt corrosion in the same temperature range /17/. Figure 42 shows the morphology of a SCRB210 specimen after corrosion and removal of the corrosion products by soaking in hot water. This figure shows the selective attack of the free silicon phase which is also a common feature in molten salt corrosion.

Aluminum melting fluxes are typically eutectic salt mixtures of KCl and NaCl (to reduce the melting point) to which small amounts of cryolite may be added. Because silicates in the Na_2O-K_2O-SiO_2 ternary system

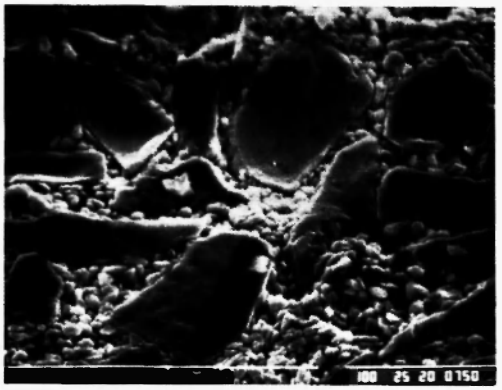

Fig. 42: Scanning electron micrograph of surface of CS101K specimen after corrosion in Ar-20%O_2-3%H_2O-0.105%KCl environment at 900°C and etching in hot water to remove corrosion products showing selective attack of free Si phase.

can have lower melting points than in either binary system, it is likely that environments containing both alkali species will be more corrosive than those containing only one. Figure 43 shows the corrosion produced on SASC at 1000°C by exposure to an environment produced by passing Ar-20%O_2-3%H_2O through a eutectic salt bath of KCl and NaCl held at 850°C. The environment containing both alkali species is more corrosive than either single species. Experiments in which small amounts (5% or less) of fluorides were added to the NaCl or KCl salt baths as NaF or KF did not produce accelerated corrosion in any environment.

D. Summary

The alkali rather than the halide is the important corrosive agent in environments which contain alkali halide vapors. The corrosion products are non-protective alkali silicates which are liquid at elevated temperatures and may flow and drip from the samples at sufficiently high temperatures. Under these conditions, the equilibrium activity of the alkali oxide in the atmosphere is the best predictor of the corrosion rate. Water vapor accelerates the corrosion while Cl_2 or HCl in the environment inhibits it. Higher rates of attack are produced in environments containing both

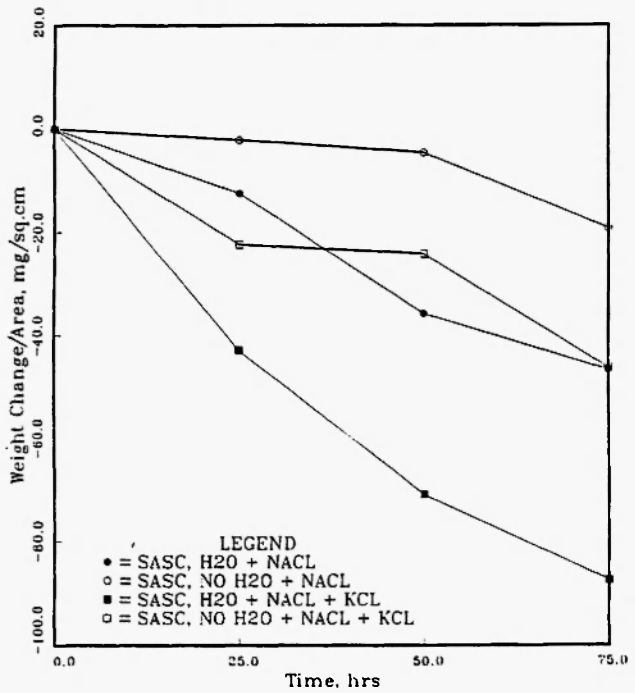

Fig. 43: Weight change results for SASC corroded at 1000°C in Ar-20%O_2-3%H_2O environment with NaCl or mixed NaCl-KCl vapor generated at 850°C showing more rapid attack in the mixed alkali environment.

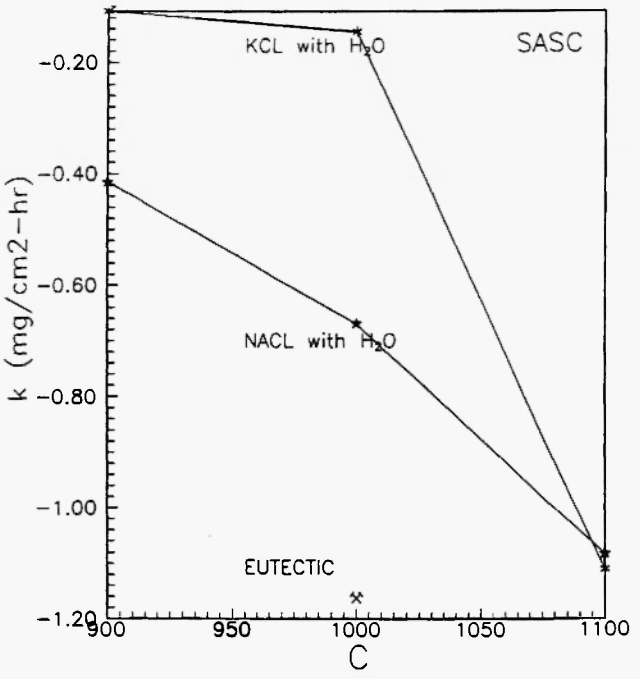

Fig. 44: Corrosion rate constants for SASC in Ar-20%O_2-3%H_2O gas mixtures between 900 and 1100°C with KCl or NaCl added from salt baths held at 850°C.

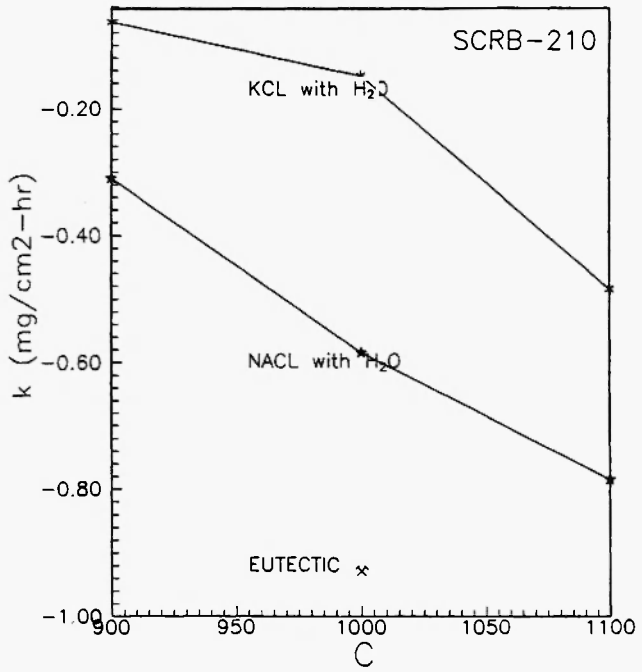

Fig. 45: Corrosion rate constants for SCRB210 in Ar-20%O_2-3%H_2O gas mixtures between 900 and 1100°C with KCl or NaCl added from salt baths held at 850°C.

sodium and potassium than in environments which contain only one alkali species. SASC is attacked at a slightly higher rate than siliconized silicon carbide, but siliconized silicon carbides are subject to selective attack of the free silicon phase.

The linear corrosion rate constants in a particular environment increase with increasing temperature. Figures 44 and 45 summarize the approximate linear corrosion rates determined in these experiments on SASC and on SCRB 210 as a function of temperature between 900 and 1100°C in environments containing 20%O_2 and 3%H_2O with additions of KCl or NaCl from salt baths held at 850°C. The corrosion rates increase by a factor of approximately two to three over this Temperature interval. The vapors produced by a eutectic salt mixture at 1000°C produce higher corrosion rates for both materials than either pure salt vapor.

ACKNOWLEDGMENT

This research was supported by the Gas Research Institute through subcontract No. GRI-TPSU-UI-1302-

390 from the Center for Advanced Materials at the Pennsylvania State University under Prime Contract No. 5084-238-1302.

REFERENCES

1. R.A. Penty and J.W. Bjerklie, "Silicon carbide for high temperature heat exchangers", *Ceramic Engineering and Science Proceedings*, **3**, 120-127 (1982).
2. W.W. Liang and E.S. Tabb, "GRI's advanced heat transfer system program", in: *Industrial Heat Exchangers*, A.J. Hayes, W.W. Liang, S.L. Richlen and E.S. Tabb (eds.), ASM International, Metals Park, OH, 1985; pp. 29-35.
3. J.A. Costello and R.E. Tressler, "Oxidation kinetics of silicon carbide crystals and ceramics", *J. Am. Ceram. Soc.*, 69, 674-681 (1986).
4. Z. Zheng, R.E. Tressler and K.E. Spear, "Oxidation of single crystal silicon carbide", *J. Electrochem. Soc.*, **137**, 854-858 (1990).
5. P.D. Miller, H.H. Krause, D.A. Vaughan and W.K. Boyd, "The mechanism in high temperature corrosion in municipal incinerators", *Corrosion*, **28**, 674-681 (1972).
6. M. van Roode, J.R. Price, R.E. Gildersleeve and C.E. Smeltzer, "Ceramic coatings for corrosive environments", *Ceramic Engineering and Science Proceedings*, 9, 1245-1259 (1988).
7. J.I. Federer and P.J. Jones, "Oxidation/Corrosion of Metallic and Ceramic Materials in Aluminum Remelt Furnaces", ORNL/TM-9741, 1985.
8. P.L. Daniel and R.A. Rapp, "Halogen corrosion of metals", *Advances in Corrosion Science and Technology*, **6**, 55-172 (1976).
9. M.J. McNallan, S.Y. Ip, S. Saam and W.W. Liang, "High temperature corrosion of SiC based ceramics in chlorine containing environments", in: *High Temperature Materials Chemistry III*, Z.A. Munir and D. Cubiciotti (eds.), The Electrochemical Society, Inc., Pennington, NJ, 1986; pp. 328-338.
10. J.E. Marra, E.R. Kreidler, N.S. Jacobson and D.S. Fox, "Reactions of silicon based ceramics in mixed oxidation-chlorination environments", *J. Am. Ceram. Soc.*, **71**, 1067-1073 (1988).
11. C. Wagner, "Passivity during oxidation of silicon at elevated temperatures", *J. Appl. Phys.*, **29**, 1295-1297 (1958).
12. J. Hinze and H.C. Graham, "The active oxidation of Si and SiC in the viscous gas flow regime", *J. Electrochem. Soc.*, **123**, 1066-1073 (1976).
13. D.S. Park, M.J. McNallan, C. Park and W.W. Liang, "Active corrosion of sintered alpha silicon carbide in oxygen-chlorine gases at elevated temperatures", *J. Am. Ceram. Soc.*, **73**, 1323-1329 (1990).
14. S.Y. Ip, M.J. McNallan and D.S. Park, "Active oxidation of SiC-based ceramics in Ar-2%Cl_2-O_2 gas mixtures at 1000°C", *J. Am. Ceram. Soc.*, **75**, 1942-1948 (1992).
15. R. Browning, J. Smialek and N.S. Jacobson, "Scanning auger microscopy of corroded SiC", *J. Mater. Sci. Lett.*, **5**, 1122-1124 (1986).
16. R. Browning, J. Smialek and N.S. Jacobson, "Multielement mapping of alpha SiC by scanning auger microscopy", *Adv. Ceram. Mater.*, **2**, 773-779 (1987).
17. N.S. Jacobson and J.L. Smialek, "Hot corrosion of sintered alpha SiC at 1000°C", *J. Am. Ceram. Soc.*, 68, 432-439 (1985).
18. H. Du, R.E. Tressler, K. Spear and C.G. Pantano, "Oxidation studies of crystalline CVD silicon nitride", *J. Electrochem. Soc.*, **136**, 1527-1536 (1989).
19. H. Du, R.E. Tressler and K. Spear, "Thermodynamics of the Si-N-O system and kinetic modelling of oxidation of Si_3N_4", *J. Electrochem. Soc.*, **136**, 3210-3215 (1989).
20. L.U.T. Ogbuji and J.L. Smialek, "Evidence from transmission electron microscopy for an oxynitride layer in oxidized Si_3N_4", *J. Electrochem. Soc.*, **138**, L51-L53 (1991).
21. P.P. Hsu, S.Y. Ip, C. Park and M.J. McNallan, "Oxidation of silicon, silicon carbide, and silicon nitride in gases containing oxygen and chlorine", *J. Am. Ceram. Soc.*, **76**, 1621-1623 (1993).
22. C. Park and M.J. McNallan, "High temperature mixed oxidation of nitride bonded silicon carbide in oxidizing gas mixtures containing 2% Cl_2", *J. Am. Ceram. Soc.*, 78, 922-928 (1995).
23. J. Monkowski, R.E. Tressler and J. Stach, "The

structure and composition of silicon oxides grown in HCl/O_2 ambients", *J. Electrochem. Soc.*, **125**, 1867-1873 (1978).

24. M.D. Monkowski, J.R. Monkowski, I.S.T. Tsong and R.E. Tressler, "Microstructure development during the thermal oxidation of silicon in chlorine containing ambients", *J. Non-Crystalline Solids*, **49**, 201-209 (1982).
25. Z. Zheng, R.E. Tressler and K.E. Spear, "The effects of Cl_2 on the oxidation of single crystal silicon carbide", *Corros. Sci.*, **33**, 557-567 (1992).
26. M. McNallan, M. Van Roode and J.R. Price, "The mechanism of high temperature corrosion of SiC in flue gases from aluminum remelting furnaces", in: *Corrosion and Corrosive Degradation of Ceramics*, M. McNallan and R.E. Tressler (eds.), American Ceramic Society, Westerville, OH, 1990; pp. 445-467.
27. N.S. Jacobson, "Corrosion of silicon based ceramics in combustion environments", *J. Am. Ceram. Soc.*, **76**, 3-28 (1993).
28. Z. Zheng, R.E. Tressler and K. Spear, "The effect of sodium contamination on the oxidation of single crystal silicon carbide", *Corros. Sci.*, **33**, 545-556 (1992).
29. Z. Zheng, R.E. Tressler and K. Spear, "A comparison of the oxidation of sodium implanted CVD Si_3N_4 with the oxidation of sodium implanted SiC crystals", *Corros. Sci.*, **3**, 569-580 (1992).
30. N.S. Jacobson, "Kinetics and mechanism of corrosion of alpha SiC by molten salts", *J. Am. Ceram. Soc.*, **69**, 74-82 (1986).
31. D.S. Fox and N.S. Jacobson, "Molton salt corrosion of silicon nitride: I. Sodium carbonate", *J. Am. Ceram. Soc.*, **71**, 128-138 (1988).
32. M.J. McNallan, S.Y. Lee and P.P. Hsu, "Oxidation of silicon based ceramics in the presence of alkali halides", *Corrosion of Advances Ceramics*, K. Nickel (ed.), Kluwer Academic Publishers, 1994; pp. 189-202.